

# Genesis of Tropical Storm Debby (2006) within an African Easterly Wave: Roles of the Bottom-Up and Midlevel Pouch Processes

LIN ZHU

*Key Laboratory of Meteorological Disaster, Ministry of Education, Nanjing University of Information Science and Technology, Nanjing, China, and Department of Atmospheric and Oceanic Science, University of Maryland, College Park, College Park, Maryland*

DA-LIN ZHANG AND STEFAN F. CECELSKI

*Department of Atmospheric and Oceanic Science, University of Maryland, College Park, College Park, Maryland*

XINYONG SHEN

*Key Laboratory of Meteorological Disaster, Ministry of Education, Nanjing University of Information Science and Technology, Nanjing, China*

(Manuscript received 24 July 2014, in final form 15 March 2015)

## ABSTRACT

The “bottom up” generation of low-level vortices (LVs) and midlevel vortices (MVs) during the genesis of Tropical Storm Debby (2006) and the roles of a midlevel “marsupial pouch” associated with an African easterly wave (AEW) are examined using an 84-h simulation with the finest grid size of 1.33 km. Results show that several MVs are generated in leading convective bands and then advected rearward into stratiform regions by front-to-rear ascending flows. Because of different Lagrangian storm-scale circulations, MVs and LVs are displaced along different paths during the early genesis stages. MVs propagate cyclonically inward within the AEW pouch while experiencing slow intensification and merging under the influence of converging flows. The MVs’ merging into a mesovortex is accelerated as they come closer to each other in the core region. In contrast, the low-level Lagrangian circulation is opened as a wave trough prior to tropical depression (TD) stage, so the LVs tend to “escape” from the pouch region. Only after the low-level flows become closed do some LVs congregate and contribute directly to Debby’s genesis. The TD stage is reached when the midlevel mesovortex and an LV are collocated with a convective zone having intense low-level convergence. Results also show the roles of upper-level warming in hydrostatically maintaining the midlevel pouch and producing mesoscale surface pressure falls. It is found that the vertically tilted AEW with a cold dome below is transformed to a deep warm-core TD vortex by subsiding motion. A conceptual model describing the key elements in the genesis of Debby is also provided.

## 1. Introduction

Tropical cyclogenesis (TCG) remains one of the challenging topics in tropical meteorology today, despite recent advances made by observational and modeling studies. The climatological and synoptic-scale conditions associated with TCG are well known, ranging from warm sea surface temperatures (SSTs) to weak

vertical wind shear (VWS; Gray 1968, 1985). What processes are responsible for TCG within African easterly waves (AEWs) after moving offshore over the Atlantic Ocean remain elusive, given the lack of high-resolution observations over the genesis regions. These waves are typically bounded latitudinally within 10°–20°N and propagate off the West African coast with diurnally active deep convection (Frank 1970; Avila and Pasch 1992; Hopsch et al. 2007, 2010; Goldenberg and Shapiro 1996). Several field campaigns have been conducted in the past few years, such as the NASA African Monsoon Multi-disciplinary Activities (NAMMA) field experiment in 2006 (Zipser et al. 2009) and the Pre-Depression Investigation

---

*Corresponding author address:* Dr. Da-Lin Zhang, Department of Atmospheric and Oceanic Science, University of Maryland, College Park, 2419 CSS Building, College Park, MD 20742.  
E-mail: dalin@atmos.umd.edu

of Cloud Systems in the Tropics (PREDICT) in 2010 (Montgomery et al. 2012), because more than half of North Atlantic tropical storms (TSs) form within AEWs.

The relationship between AEWs and the associated processes leading to TCG has been the focal point of numerous observational and modeling studies. Thorncroft and Hodges (2001), Hopsch et al. (2007), and Ross and Krishnamurti (2007) have shown two predominant tracks for AEWs: one on the northern side and the other on the southern side of an African easterly jet (AEJ), typically located near 15°N, both of which have implications for TCG (Chen et al. 2008; Zawislak and Zipser 2010). Ross et al. (2009) and Cornforth et al. (2009) showed the important roles of barotropic energy conversion and diabatic heating in the growth of AEWs, which in turn preconditions an environment for TCG. Emphasizing the role of AEWs in TCG, Dunkerton et al. (2009) postulated that mesovortices and deep convection tend to be generated near the AEW critical latitude. Later, Montgomery et al. (2010) and Wang et al. (2010) elaborated on the concept of a “marsupial pouch” near the intersection of the AEW trough axis and critical latitude. Within this pouch region, TCG is favored as moist air parcels remain within a closed Lagrangian circulation of the AEW and, thus, are protected from adverse environmental conditions such as dry air in the Saharan air layer (SAL). The wave pouch also facilitates vorticity aggregation and convective organization leading to TCG (Wang 2012, 2014).

Most of the previous studies investigating TCG have mainly focused on the low- to midlevel processes, especially the growth of cyclonic vorticity in the lower troposphere, the so-called bottom-up growth of meso- $\beta$ -scale vortices (e.g., Zhang and Bao 1996; Montgomery et al. 2012; Wang et al. 2010). The warm-core development is a fundamental character of a mature tropical cyclone (TC; Ritchie and Holland 1997; Houze et al. 2009). The upper-tropospheric warming during TCG just becomes a topic of studies (e.g., Zhang and Zhu 2012; Cecelski and Zhang 2013; Cecelski et al. 2014). Zhang and Zhu (2012) showed that the upper-level warming by compensating subsidence and the residual between diabatic heating and adiabatic cooling in updraft regions account hydrostatically for meso- $\alpha$ -scale falls in mean sea level pressure (MSLP) associated with a developing tropical depression (TD). Cecelski and Zhang’s (2013) work further elaborated on the importance of upper-level processes in TCG, demonstrating the relationship between deep convection, the convectively generated upper-level outflow, and storm-scale warming.

Several recent studies have been conducted to investigate the genesis of TS Debby (2006), which

occurred during the NAMMA campaign (Chiao and Jenkins 2010; Sippel et al. 2011; Lin et al. 2013). Lin et al. (2013) found that the origin of a pre-Debby mesoscale convective system (MCS) could be traced back to an area to the southwest of the Arabian Peninsula, Asir Mountains, and Ethiopian highlands. Chiao and Jenkins (2010) showed the importance of the Guinea highlands in the formation of the AEW by modulating the impinging westerly flow to enhance the cyclonic circulation. Sippel et al. (2011) used ensemble simulations to reveal that dry air in the SAL slowed Debby’s intensification during the pre-TD and TD stages, while cold SSTs and large VWS were responsible for Debby’s dissipation thereafter. Despite the previous studies of the case, it still remains unclear what physical processes have led to the genesis of Debby.

Thus, the objectives of this study are (i) to document the evolution of an AEW in which Debby was spawned and the environmental conditions that were favorable for TCG; (ii) to examine the formation and amplification of several meso- $\beta$ -scale midlevel (700–500 hPa) vortices (MVs) and their merging and interaction with meso- $\beta$ -scale low-level (below 700 hPa) vortices (LVs; Cecelski and Zhang 2013) leading to the genesis of Debby; and (iii) to investigate the roles of bottom-up growth, wave pouch, and upper-level processes in the genesis of Debby. They are achieved using the best-track, satellite image, the National Centers for Environmental Prediction (NCEP) final analysis, and an 84-h triply nested-grid Weather Research and Forecast (WRF) Model simulation with the finest grid size of 1.33 km.

The next section provides an overview of the case. Section 3 describes the major WRF Model configuration and verification of the WRF simulation against available observations. Section 4 presents the physical processes leading to the genesis of Debby, including the development of the upper-level warming in relation to meso- $\alpha$ -scale MSLP falls, the bottom-up development of some LVs and their “escape” from the pouch region, as well as the importance of merging MVs and subsequent coupling with LVs within the AEW pouch in TCG. Piecewise potential vorticity (PV) inversion will be used to infer the contribution of the MVs to the surface MSLP fall. Section 5 examines thermodynamic transformation during the genesis of Debby. A schematic TCG model for the present case is given in the final section.

## 2. Overview

According to the official report of the National Hurricane Center (NHC), the genesis of Debby occurred

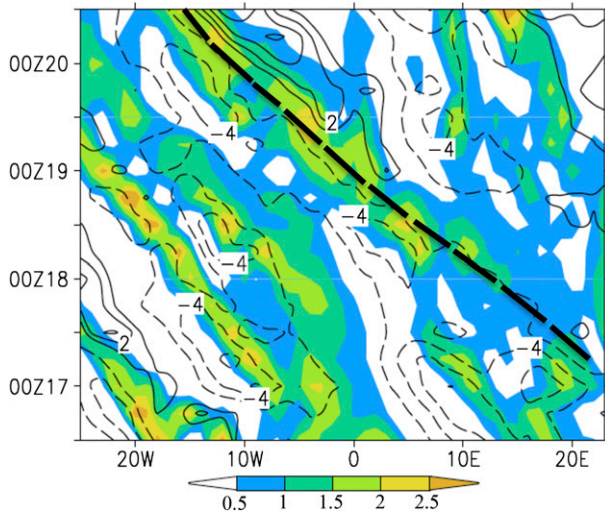


FIG. 1. Hovmöller diagram of the meridionally ( $5^{\circ}$ – $15^{\circ}$ N) averaged cyclonic relative vorticity (shaded;  $10^{-5} \text{ s}^{-1}$ ), superimposed with meridional wind speeds (dashed; interval of  $2 \text{ m s}^{-1}$ ) at 600 hPa during the period from 1200 UTC 16 Aug to 1200 UTC 20 Aug 2006 and longitudinally spanning from  $20^{\circ}$ W to  $25^{\circ}$ E, based on the NCEP final analysis. The thick dashed line represents the trough axis of the AEW under study.

as a result of “convective banding” within a broad closed circulation of an AEW. This AEW could be traced back to 1200 UTC 16 August 2006 when its first signal appeared on the leeward side of the Darfur mountains (Lin et al. 2013), located roughly at  $20^{\circ}$ E, with the peak relative vorticity of  $10^{-5} \text{ s}^{-1}$  at 600 hPa (Fig. 1). The AEW propagated westward at approximately  $8 \text{ m s}^{-1}$ , which is used as the phase speed for the comoving reference frame and streamline analyses shown in the following sections. The AEW intensified slowly, as indicated by its mean vorticity, as it moved westward and exhibited a southerly flow in its eastern quadrant after 0000 UTC 19 August 2006 (Figs. 1 and 2a). A meso–low pressure area formed within the AEW shortly after moving off the West African coast at 0000 UTC 21 August 2006, with the coupled AEW–mesolow system moving northwestward beyond  $15^{\circ}$ N (not shown). As a result, the tracking of both systems shifts preferentially to the mesolow after 0000 UTC 21 August 2006. The mesolow was finally declared TD Debby near  $11.6^{\circ}$ N,  $21.7^{\circ}$ W at 1800 UTC 21 August and became a TS at 0000 UTC 23 August 2006 (Franklin 2006). Debby failed to intensify further as a result of entraining dry air from the SAL (Sippel et al. 2011). A day later, Debby reintensified as a result of increased deep convection near the AEW center. Even with the increased convective activity, Debby’s intensification was brief because of an increased VWS and cool SSTs disrupting the persistence of deep convection near the storm center.

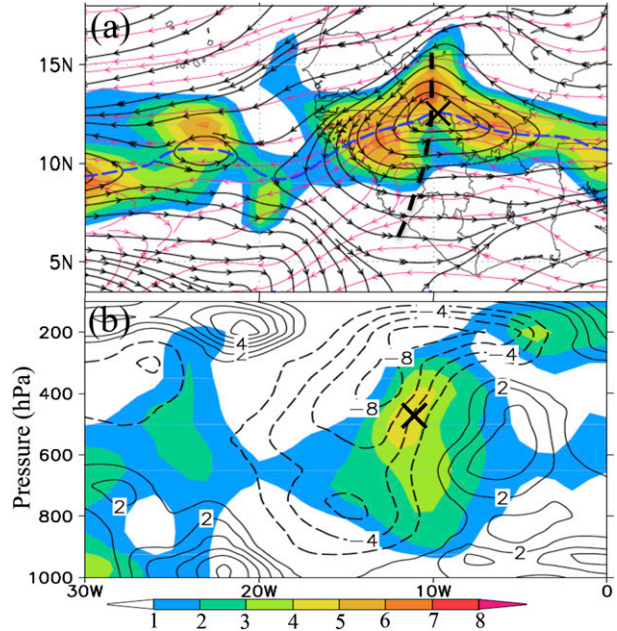


FIG. 2. (a) Horizontal distribution of the cyclonic relative vorticity (shaded;  $10^{-5} \text{ s}^{-1}$ ), superimposed with the comoving (black) and ground-relative (red) streamlines at 600 hPa; and (b) west–east vertical cross section of the zonal-mean ( $5^{\circ}$ – $15^{\circ}$ N) cyclonic relative vorticity (shaded;  $10^{-5} \text{ s}^{-1}$ ) and meridional wind speeds (contours; interval of  $2 \text{ m s}^{-1}$ ; solid is southerly; dashed is northerly) at the model initial time (0000 UTC 20 Aug 2006). The blue and thick black dashed curves in (a) denote the critical latitude and trough axis, respectively. The  $\times$  symbol shows the location of the AEW under study.

This weakening continued, and the disturbance was weakened to a remnant low pressure disturbance at 1200 UTC 26 August 2006 (not shown).

Figures 2 and 3 show some synoptic-scale features of the AEW that were favorable for TCG at 0000 UTC 20 August 2006, which is the model initial time used for the present study. A zonally distributed cyclonic vorticity belt, mostly shear related, was centered at  $10^{\circ}$ N, with several mesoscale concentrated vorticity regions in the easterly flow; this belt coincided well with zonally distributed convective activity in satellite imagery (not shown). The pouch associated with the AEW was located near  $12.3^{\circ}$ N,  $10^{\circ}$ W along the trough axis, as evidenced by the comoving closed streamlines (Fig. 2a), with the pouch center marked by a cross. As will be shown later, TCG took place in the AEW pouch after moving offshore. A meridionally ( $5^{\circ}$ – $15^{\circ}$ N) averaged zonal cross section shows a coherent near-upright cyclonic vorticity column associated with the AEW pouch, with a deep layer of cyclonic circulation and relatively weak VWS at a zonal scale of about 2000 km (Fig. 2b).

Meridional cross sections show a northward-tilted cyclonic vorticity column of the AEW (Fig. 3a) peaked

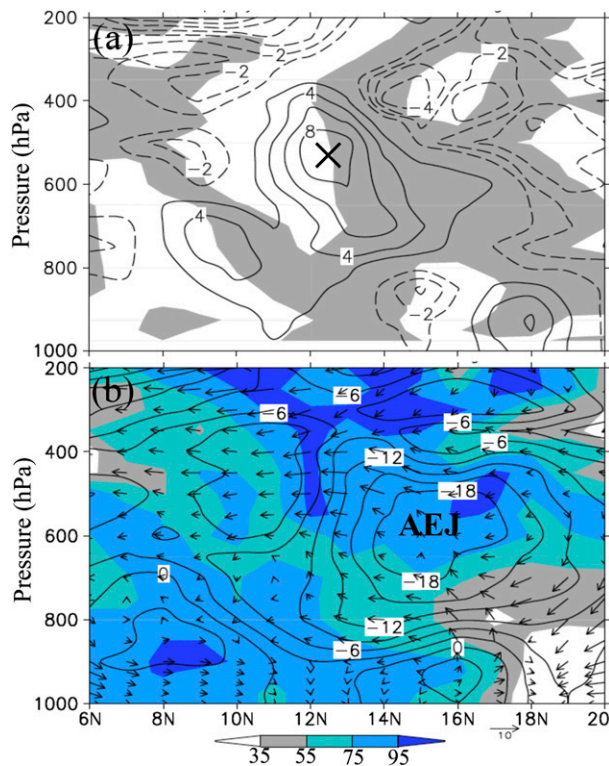


FIG. 3. North-south ( $6^{\circ}$ – $20^{\circ}$ N) cross section along  $10.5^{\circ}$ W of (a) the meridional PV gradient (shaded for negative values;  $\text{PVU km}^{-1}$ ) and relative vorticity (solid is positive; dashed is negative;  $10^{-5} \text{ s}^{-1}$ ) from the NCEP final analysis at 0000 UTC 20 Aug 2006. The  $\times$  symbol represents the peak relative vorticity of the AEW under study. (b) Relative humidity (shaded; %) and zonal wind speeds (contours; interval of  $3 \text{ m s}^{-1}$ ) superimposed with in-plane flow vectors.

near 500 hPa, with PV gradients reversed from positive to negative while heading north. The reversed meridional PV gradients indicate the presence of combined barotropic–baroclinic instability (Charney and Stern 1962; Norquist et al. 1977), which is indicative of an imminent TCG event (Molinari et al. 1997, 2000). This instability was complemented by strong shear-generated vorticity associated with an AEWJ having zonal winds in excess of  $18 \text{ m s}^{-1}$  to the north of the AEW (Fig. 3b). Obviously, the AEWJ was a source of dynamical instability for the AEW, which itself was sustained by the significant meridional temperature gradients in the lower troposphere.

Figure 3b also shows large north-south moisture gradients at 0000 UTC 20 August 2006, with substantially dry air to the north of the AEW as an outbreak of the SAL dust took place. The relative humidity (RH) in excess of 75% appeared within the AEW pouch. With the presence of an intense high pressure system (i.e., as an extension of the Azores high) to the north of the

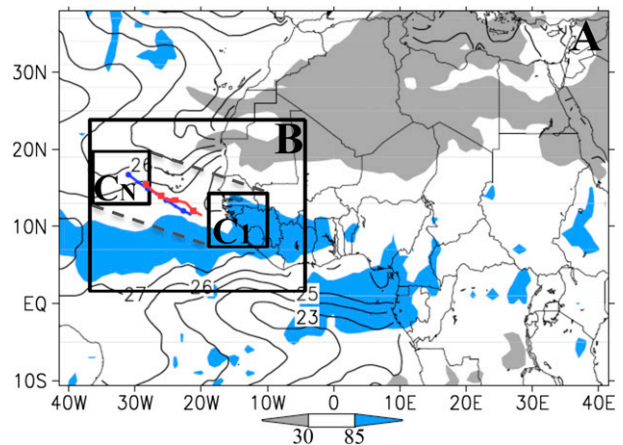


FIG. 4. Horizontal distribution of relative humidity (gray is dry; blue is moist; %) and sea surface temperature (contours; interval of  $1^{\circ}\text{C}$ ) from the NCEP final analysis at the model initial time. The model meshes with horizontal resolutions of 12 (A), 4 (B), and 1.33 km (C) are overlaid. Domain C follows the movement of the storm, and  $C_1$  and  $C_N$  denote the first and the last position of domain C, respectively. The simulated (red) and observed (blue) storm tracks during the 84-h simulations are superimposed.

AEW (not shown), the large-scale flow pattern favored the entrainment of dry air from the north into the AEW circulation, possibly delaying TCG. Furthermore, the large-scale flow pattern tended to steer the developing disturbance to the northwest, toward the Cape Verde Islands, instead of westward toward warmer SSTs.

Despite the presence of several favorable large-scale conditions, it is still unclear what mesoscale processes lead to the genesis of Debby. Most importantly, what are the roles of the AEW, convectively generated vortices, and their interactions in TCG? To help answer this question, we invoke an analysis of a cloud-resolving model simulation of the storm, as described in the following three sections.

### 3. Model description and verification

In this study, a two-way interactive, movable, triply nested version of the nonhydrostatic Advanced Research WRF Model (WRF-ARW V3.0; Skamarock et al. 2008) is used to simulate the genesis of TS Debby. The triply nested domains have  $x$ - $y$  dimensions of  $168 \times 285$  (A),  $650 \times 650$  (B), and  $455 \times 455$  (C), with the grid spacing of 12, 4, and 1.33 km, respectively (Fig. 4). The model parameterization schemes employed for the 12- and 4-km resolution domains are (i) the Thompson three-ice cloud microphysics scheme (Thompson et al. 2004, 2008); (ii) the Yonsei University planetary boundary layer (PBL) parameterization with the Monin–Obukhov surface-layer scheme (Hong et al. 2006); (iii) the Rapid

Radiative Transfer Model (RRTM) longwave radiation scheme with six molecular species (Mlawer et al. 1997), and the Dudhia shortwave radiation scheme; and (iv) a modified version of the Kain–Fritsch cumulus parameterization scheme (Kain 2004). The 1.33-km domain uses the same schemes as the outer two domains, with the exception of cumulus parameterization as deep convection is resolved explicitly within this domain. We use 35 vertical sigma levels  $\sigma$ ,<sup>1</sup> with the model top set at 50 hPa.

Domains A and B are initialized at 0000 and 1200 UTC 19 August 2006, respectively, and they are integrated forward through analysis nudging for the respective 24- and 12-h periods until 0000 UTC 20 August 2006, at which time domain C is initialized, 48 h prior to Debby's TD stage. All three domains are then integrated for an additional 84 h [i.e., 1200 UTC 23 August 2006 (84 h)], which is 12 h after Debby enters its TS stage. Such an integration method is used to minimize computational costs while creating an improved large-scale analysis for the initialization of the high-resolution nest. Once initialized, domain C is moved within domain B every 10 min following the storm center. Given the lack of a distinguishable MSLP disturbance for the majority of the integration period, the 1.33-km domain must be moved manually using prescribed steps. The model initial conditions and the outermost lateral boundary conditions are obtained from NCEP's final analysis, with the latter updated every 6 h throughout the integration. Additionally, constant SSTs from the model initial time are used during the 84-h simulation, as minimal changes in SSTs took place over the length of the simulation.

In general, the WRF simulation reasonably reproduces the large-scale circulations in which Debby is generated (not shown). So the following only validates the mesoscale structures and evolution of the simulated storm against available observations. First, WRF simulates reasonably well the track of Debby as compared to the NHC estimates (Franklin 2006), including the timing and location of TCG (Figs. 4 and 5). However, the simulated storm moves slower than the observed during the final 12-h integration, generating a track error of about 120 km at the end of the 84-h simulation.

The simulated storm intensity also compares favorably to the observed in terms of the central

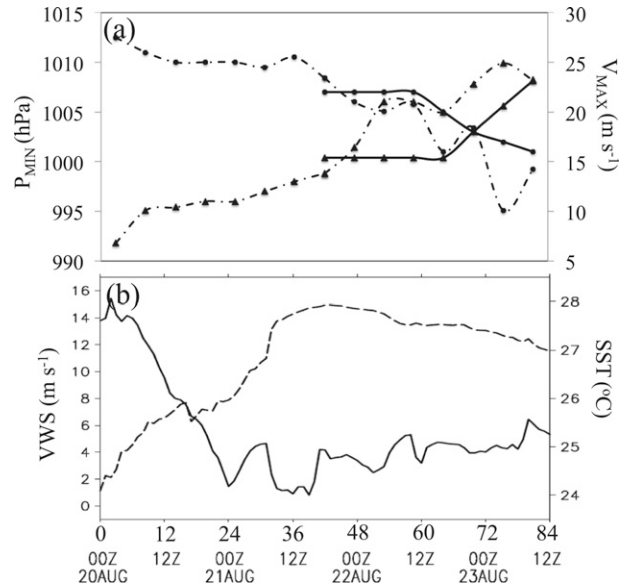


FIG. 5. (a) Time series (6-h interval) of the simulated (dotted-dashed; from the 12-km-resolution domain) vs observed (solid) minimum sea level pressure (dots; hPa) and maximum surface winds (triangles;  $\text{m s}^{-1}$ ) during the 84-h simulation, valid from 0000 UTC 20 Aug to 1200 UTC 23 Aug 2006. Note that the best track is only available during the final 36 h. (b) Hourly time series of vertical wind shear (solid;  $\text{m s}^{-1}$ ) between 200 and 850 hPa and SSTs (dashed;  $^{\circ}\text{C}$ ), estimated using an area of  $600 \text{ km} \times 600 \text{ km}$  centered on the surface circulation center.

minimum pressures  $P_{\text{MIN}}$ , although it is, on average, slightly stronger than the best estimates after 1800 UTC 21 August 2006 (42 h) in terms of the maximum surface wind  $V_{\text{MAX}}$  (Fig. 5a). Of interest is that both the simulated and observed  $P_{\text{MIN}}$  remain nearly constant above 1000 hPa during the TCG period, even after the observed disturbance was named a TS at 0000 UTC 23 August 2006 by the NHC. We may state that the WRF simulation captures the evolution of Debby's major stages, with the modeled TD occurring at 0000 UTC 22 August 2006 (48 h), at which time a closed surface isobar, plotted with a 4-hPa interval, develops. That is, in the hours prior to being declared a TD, the simulated storm has little appreciable MSLP fall, with a constant  $P_{\text{MIN}}$  of 1009 hPa prior to 1200 UTC 21 August 2006 (36 h). Subsequently, TCG occurs in both the observations and simulation as the 200–850-hPa VWS decreases from 15 to  $3 \text{ m s}^{-1}$ , complemented by an increase of SSTs to near  $28^{\circ}\text{C}$  (Fig. 5b). In addition to the deepening of the MSLP disturbance, both the simulation and best estimates depict a steady rise in  $V_{\text{MAX}}$  (i.e., at a rate of about  $8 \text{ m s}^{-1}$  in 18 h) over the same period until 1200 UTC 23 August 2006 (84 h) (Fig. 5a). However, the model produces higher values in local  $V_{\text{MAX}}$  during the 42–60-h simulation. Nevertheless,

<sup>1</sup>The 35  $\sigma$  levels are given as follows: 1, 0.992 93, 0.985 31, 0.976 58, 0.966 19, 0.953 61, 0.936 67, 0.914 46, 0.887 31, 0.855 58, 0.819 74, 0.780 26, 0.737 68, 0.692 58, 0.645 53, 0.597 12, 0.544 31, 0.488 51, 0.431 14, 0.373 62, 0.317 26, 0.267 47, 0.223 63, 0.185 16, 0.151 53, 0.122 23, 0.096 83, 0.074 9, 0.056 05, 0.041, 0.031, 0.022, 0.013, 0.007, 0.003, and 0.

little differences in intensity occur between the simulation and observations at the end of the 84-h simulations.

Because the direct observations of the storm structures during TCG are not available, we compare indirectly the simulated equivalent potential temperatures  $\theta_e$  and ground-relative horizontal wind field at 950 hPa along with the outgoing long wave radiation (OLR) to the observed infrared (IR) image from the Cooperative Institute for Meteorological Satellite Studies (CIMSS) during the 84-h integration period (Fig. 6). The simulated OLR structures compare favorably to the cloud patterns of the observed. Namely, at 0000 UTC 21 August 2006 (24 h), the simulation depicts the development of two MCSs that occupy the northwestern and southeastern semicircles of the AEW, respectively. It is worth noting that only the linear MCS with a near-circular cloud pattern in the southeastern semicircle is associated with the pre-Debby disturbance progressing off the West African coast. Although the simulated northwestern MCS differs somewhat from the observed in terms of location and shape, it weakens with time as a result of the intrusion of low- $\theta_e$  air from northwest, as will be discussed later. The linear MCS associated with the pre-Debby disturbance appears to be in reasonable agreement in terms of the timing and location with that seen in satellite imagery (cf. Figs. 6a and 6d). The evolution of this MCS and convectively generated vortices within are important for the genesis of Debby, as shown in the next section. By 0600 UTC 22 August 2006 (54 h), the simulated disturbance (now TS Debby) exhibits a coherent round-shaped cloud structure near the circulation center, whose shape and size are both comparable to the observed structure (cf. Figs. 6b and 6e), indicative of development of a midlevel mesovortex. In addition, the WRF Model captures more cloud development to the south of Debby, forming cloud bands, whereas convective development to the north-northwest of Debby are suppressed because of the intrusion of dry SAL air, as indicated by lower  $\theta_e$  values. At 0000 UTC 23 August 2006 (72 h) (cf. Figs. 6c and 6f), the simulation continues to reasonably represent the round-shaped cloud patterns of TS Debby as the storm becomes completely surrounded by dry air. The cloud bands to the south tend to depart from Debby's circulation, thus contributing less and less to the further development of the storm.

#### 4. Genesis of Debby within the AEW

Given that the simulated storm is a reasonable representation of the observed Debby, we may use the cloud-resolving simulation data to investigate the mesoscale processes leading to the genesis of Debby. In this

section, we focus on the development of MVs, their relation to LVs and deep convection, and the subsequent merging within the parent AEW during the genesis of Debby.

Since there are two distinct characteristic spatial scales between Debby and its parent AEW, we plot in Figs. 7a and 7b the time–height cross sections of the respective  $600 \text{ km} \times 600 \text{ km}$  (which is close to the horizontal domain size used in Fig. 8) and  $200 \text{ km} \times 200 \text{ km}$  area-averaged relative vorticity and RH surrounding the pouch/storm during the 84-h simulation period. Obviously, the AEW provides a favorable environment for TCG, in which pronounced rotation in the 2–5-km layer is present in conjunction with sufficient lower- and midtropospheric moisture (e.g., RH values greater than 80%), as also shown in Figs. 2 and 3. As VWS decreases to less than  $6 \text{ m s}^{-1}$ , convection is able to more efficiently precondition tropospheric columns and midlevel RH increases above 90% until 0000 UTC 22 August 2006 (48 h) (Fig. 7a). With the sufficient tropospheric moistening, weak tropospheric VWS, and a distinct midlevel pouch associated with the AEW, favorable conditions exist for the genesis of Debby (Nolan 2007; Dunkerton et al. 2009; Montgomery et al. 2010; Wang et al. 2010; Cecelski and Zhang 2013). The AEW-scale midlevel cyclonic vorticity, which peaked at 3-km altitude initially and then elevated to near 4 km, increases from about  $2 \times 10^{-5}$  to  $6 \times 10^{-5} \text{ s}^{-1}$  during the first 72 h (i.e., until after entering the TS stage). Despite the AEW's favorable conditions, the subsequent deepening of Debby is slow as the SAL dry air erodes from the north-northwest (see Figs. 6e,f herein and Figs. 11a and 17 in Sippel et al. 2011), as indicated by reduced RH near 2-km altitude after 48 h into the integration. It intrudes into the developing Debby later, accounting for the subsequent slow intensity changes of the storm (cf. Figs. 7a and 5a).

At the storm scale, Fig. 7b shows the evolution of relative vorticity and RH associated with Debby in the core region of the AEW. It is evident that Debby's vorticity is higher in the midtroposphere, being associated mainly with the AEW during its pre-TD stage, with the peak cyclonic vorticity lowering in elevation thereafter (cf. Figs. 7a and 7b). This implies that Debby and its parent AEW system may attain their midlevel vorticity with a similar mechanism: namely, through stretching of the preexisting midlevel absolute vorticity. However, the storm's cyclonic vorticity becomes more concentrated in the lower layers after TD: namely, from height  $z = 4 \text{ km}$  at 1800 UTC 21 August 2006 (42 h) to the lowest 1-km layer at 1200 UTC 23 August 2006 (84 h), which is consistent with the results of Zhang and Bao (1996) and Wang (2012). During this period, its

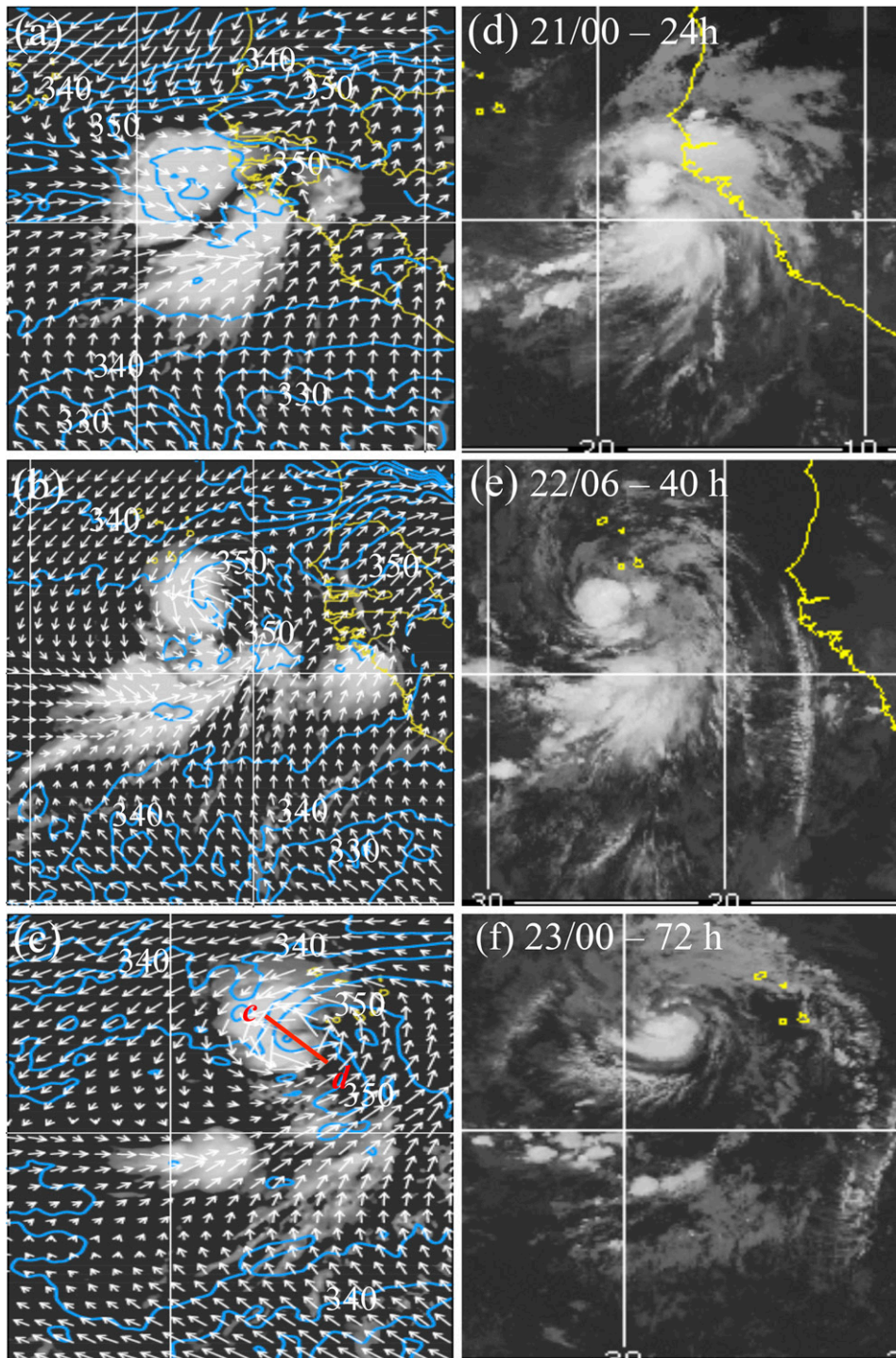


FIG. 6. Comparison of (a)–(c) the model-simulated OLR (shaded),  $\theta_e$  (contours; interval of 5 K), and horizontal wind vectors at 950 hPa with (d)–(f) the corresponding satellite IR images at (a),(d) 0000 UTC 21 Aug; (b),(e) 0600 UTC 22 Aug; and (c),(f) 0000 UTC 23 Aug 2006. Line c–d in (c) is used for the vertical cross section in Fig. 13c.

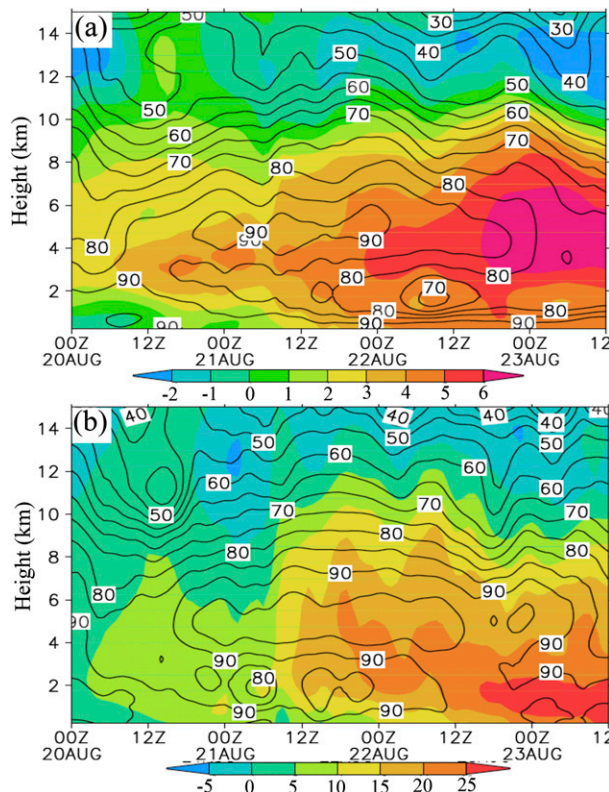


FIG. 7. Time–height cross section of the relative vorticity (shaded;  $10^{-5} \text{ s}^{-1}$ ) with relative humidity (contours; interval of 5%) overlaid using a (a)  $600 \text{ km} \times 600 \text{ km}$  area average, and (b)  $200 \text{ km} \times 200 \text{ km}$  area average (see the area coverage in Figs. 8 and 9) at the AEW pouch center during the 84-h simulations, valid from 0000 UTC 20 Aug to 1200 UTC 23 Aug 2006. Note the different color bars used for (a) and (b).

amplitude increases to more than  $2.5 \times 10^{-4} \text{ s}^{-1}$ , which is more than 4 times greater than that of the AEW in which Debby is incubated. As will be shown later, this vorticity growth is associated with some LVs in the AEW pouch region after TD, and it is consistent with the bottom-up growth of cyclonic vorticity, as shown by Zhang and Bao (1996), Hendricks et al. (2004), and Montgomery et al. (2006). Figure 7b also shows higher moisture content than that at the AEW scale, which is peaked ( $\text{RH} > 90\%$ ) in the midtroposphere. This suggests that the pouch center can more effectively retain moisture than outer regions or less susceptible to the impact of dry-air intrusion (Wang 2012). The midlevel moistening results from the upward transport of moisture by enhanced updrafts within the MCS, supporting the notion that a moist midtroposphere is a necessary condition for TCG (Nolan 2007; Hogsett and Zhang 2011; Wang 2012). The dry-air intrusion in the layer centered at 2-km altitude is evident during most of the TCG period, accounting partly for the slow genesis of Debby (Fig. 5a), despite the presence of weak VWS.

Like the AEW-scale RH, the SAL dry air has surrounded the core region (see Fig. 1e in Sippel et al. 2011), reducing the midlevel moisture after Debby reaches its TS stage.

Next, we show that the midlevel and lower-level vorticity growths shown in Figs. 7a and 7b, though convectively driven, are more determined by the evolution of the associated meso- $\beta$ -scale vortices within the AEW pouch. Figures 8a–c show the precipitation distribution of the pre-Debby MCS in the southern portion of the AEW (with a closed circulation in the ground-relative framework) at three times that are more than 24 h prior to Debby’s TD stage. The weakening of a convective band in the northwest is also evident, as shown in Fig. 6a. The pre-Debby MCS having a circular-shaped high-reflectivity ( $>35 \text{ dBZ}$ ) region near the AEW’s core is long lived, as a result of the presence of an elongated persistent confluence zone with intersecting streamlines (implying convergence) to the east feeding higher- $\theta_e$  air in the PBL into convective regions. A significant portion of stratiform rainfall (i.e., with the radar reflectivity of less than  $25 \text{ dBZ}$ ) surrounds individual convective rainfall regions. Pronounced convergence in the southerly flows, which must be associated with convection, also appears at 600 hPa (Figs. 8d–f). As can be expected, intense LVs are generated via vortex stretching in the leading convergence zone, where intense updrafts take place (cf. Figs. 8a–c and 8d–f).

Of importance is the development of meso- $\beta$ -scale MVs that are correlated with convective rainfall centers, albeit with some phase shifts; their intensities are much weaker than those of the LVs, especially near the AEW’s core region. These elevated vortices are convectively generated, and can be traced in time based on the conservation of absolute vorticity. To elucidate their development, three MVs, labeled as “A,” “B,” and “C,” are selected, all of which have a peak relative cyclonic vorticity of greater than  $3 \times 10^{-4} \text{ s}^{-1}$ , about 5–8 times larger than that of the AEW (cf. Figs. 8d–f and 2a). They appear to originate from different portions of the AEW: MV A near the AEW’s core, MV B at the middle portion of the linear MCS, and MV C from the MCS in the northwestern semicircle (Fig. 8d). It is evident that they are somewhat phase shifted during their intensifications from the corresponding LVs, with intense rainfall centers located between. Because of their distinct intensities at this early stage, the three MVs tend to absorb those nearby small and weak ones that are subsequently generated individual convective cells in the MCS.

To see the vertical structures of the MVs, Figs. 8g–i present vertical cross sections through the centers of MV

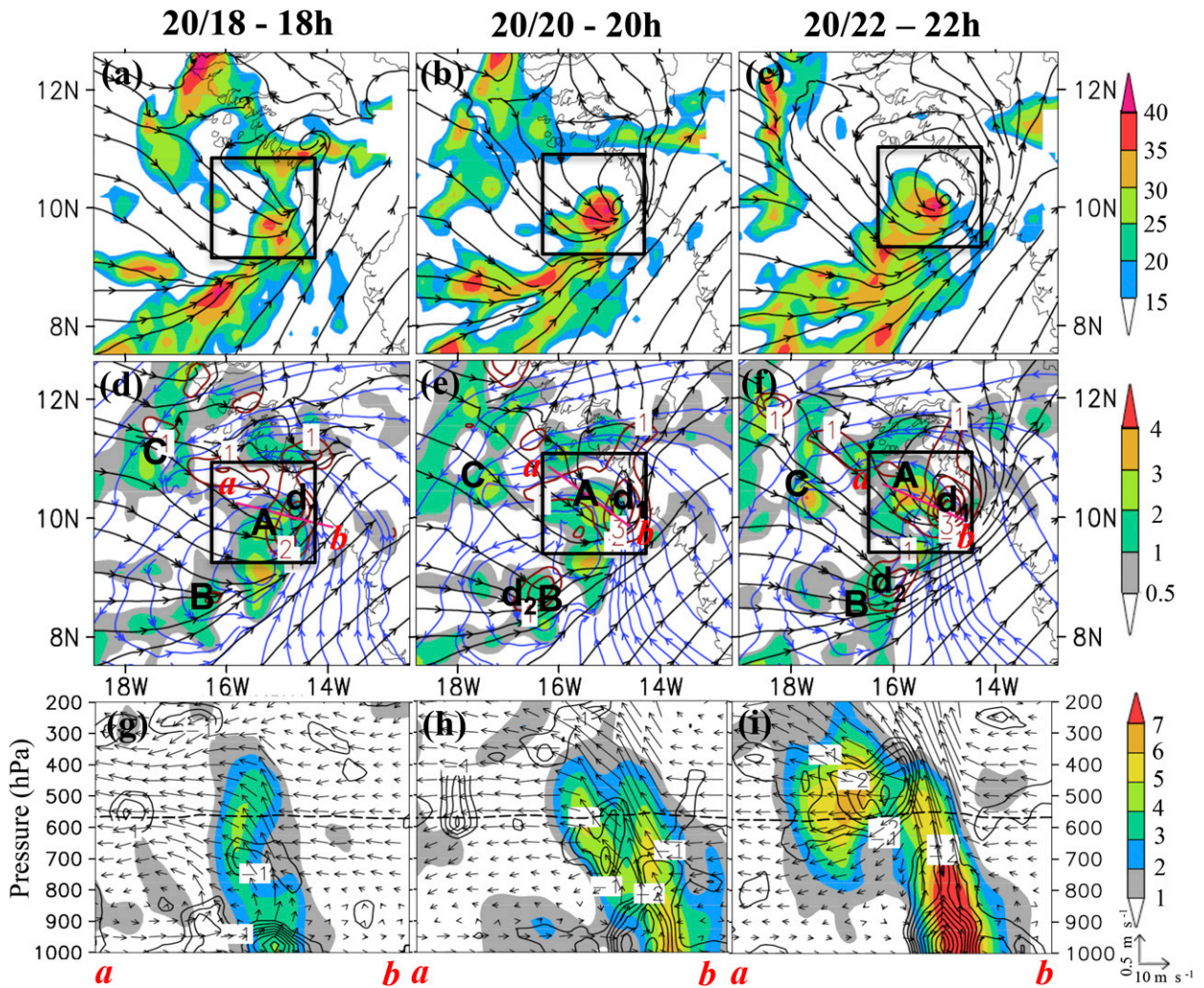


FIG. 8. (a)–(c) Horizontal distribution of radar reflectivity (shaded) and ground-relative streamlines at 950 hPa. (d)–(f) Horizontal distribution of relative vorticity ( $10^{-4} \text{ s}^{-1}$ ) at 600 (shaded) and 950 hPa (brown contours) with comoving streamlines at 600 (blue) and 950 hPa (black) overlaid. Symbols  $d_1$  and  $d_2$  denote the LVs that escape from the AEW pouch region. (g)–(i) Vertical cross section of relative vorticity (shaded;  $10^{-4} \text{ s}^{-1}$ ), divergence (contours; interval of  $5 \times 10^{-5} \text{ s}^{-1}$ ), and in-plane flow vectors along line a–b in (d)–(f) from the (left) 18-, (middle) 20-, and (right) 22-h simulations. The inner box denotes the  $200 \text{ km} \times 200 \text{ km}$  area coverage used to calculate the area-averaged variables in Fig. 7b.

A and a corresponding LV, which are both intensifying with time. The LV spins up as a result of amplifying convergence in the PBL at 1800 UTC 20 August 2006 (18h) that thickens up to 650 hPa at 2200 UTC 20 August 2006 (22h). Concurrently, updrafts of 2–3  $\text{m s}^{-1}$  intensify, fed by converging moist southwesterly flows, while the MV A grows in the front-to-rear ascending flow from the leading convective to the trailing stratiform regions. Figure 8g indicates that the MV A’s vorticity is generated in the leading updrafts below the melting level via stretching, as can be inferred from the convergence below and divergence aloft, and is then advected rearward by the front-to-rear ascending flow into the stratiform region. Of course, the preexisting

cyclonic vorticity, as shown in Figs. 1 and 2, must contribute to the vortex stretching. The front-to-rear ascending flow and the lower-level rear-to-front inflow are similar to those seen in midlatitude squall lines (Houze et al. 1989; Zhang and Gao 1989; Biggerstaff and Houze 1991), except for the rear-to-front flow that is ground based rather than elevated. Thus, the rearward transport of cloud hydrometeors in the leading convective region contributes to the formation of stratiform precipitation in accordance with the previous studies of midlatitude MCSs. Calculation of the vorticity budget indicates that vortex stretching is greater than tilting in generating both the LVs and MVs (not shown), since both the large-scale (Fig. 5b) and storm-scale VWSs become relatively

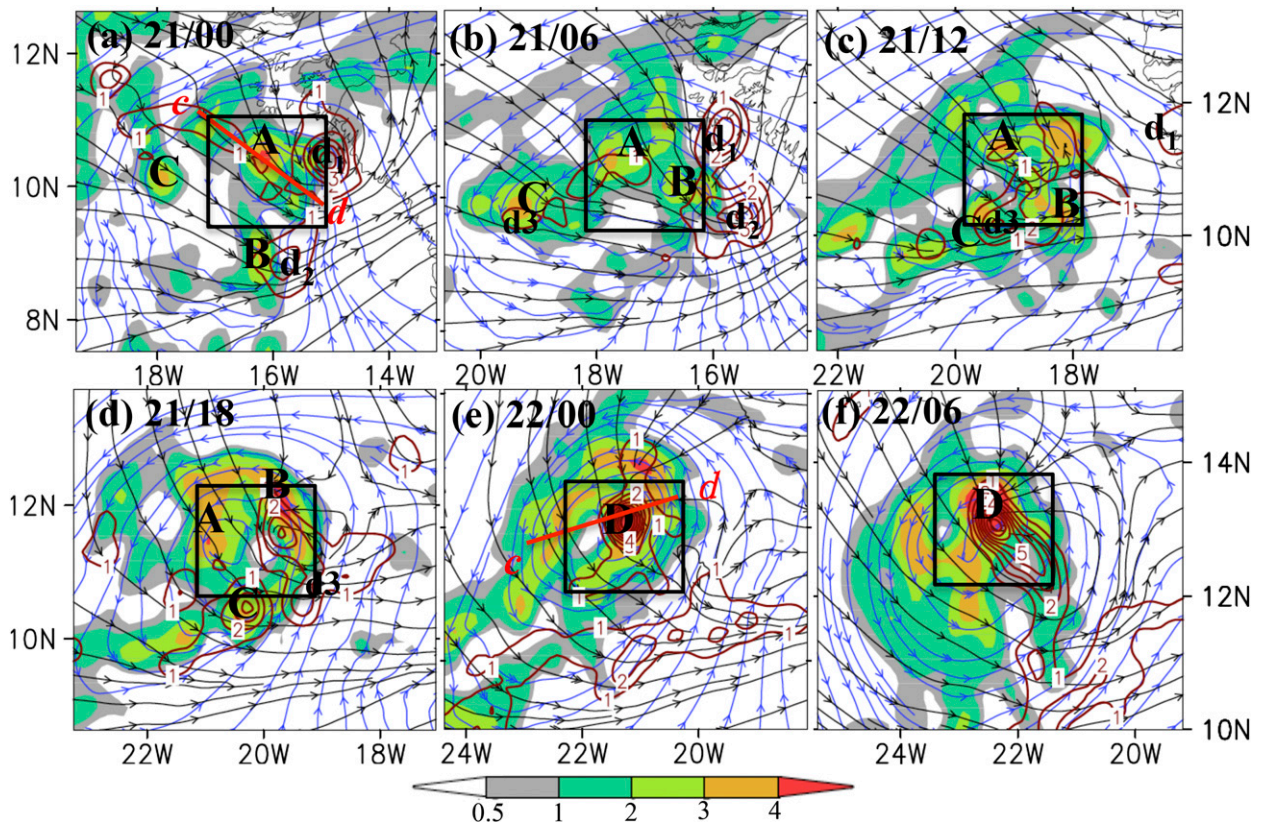


FIG. 9. As in Figs. 8d–f, except from the (a) 24-, (b) 30-, (c) 36-, (d) 42-, (e) 48-, and (f) 54-h simulations. Symbols  $d_1$ ,  $d_2$ , and  $d_3$  denote the LVs that eventually escaped from the AEW pouch region. Line c–d in (a) and (e) is used for the vertical cross section in Figs. 13a and 13b, respectively.

weak after 1800 UTC 20 August 2006 (18 h). In fact, one can see that MV A at this early stage coincides with an elevated ascending flow in the trailing stratiform region, with a separate convergence zone from that along the leading LV (Figs. 8h,i). MV A keeps intensifying moderately above the melting level, where intense convergence occurs as a result of upward motion above downward motion, which is enhanced by freezing above melting (Figs. 8h,i). This feature is similar to that observed during the genesis of Hurricane Ophelia (2005) by Houze et al. (2009). In addition, they noted that the low- to midlevel vorticity generated in convective updrafts was advected into a stratiform region attached to the leading convective cells, similar to the circumstance within (Figs. 8g–i).

It is important to note that the low-level comoving streamline patterns (contours in black) differ from those of the midlevel pouch (contours in blue) in terms of shape and orientation. Specifically, the former are opened as a wave trough to the northwest at 1800 UTC 20 August 2006 (18 h) (Fig. 8d) and to the north after 2000 UTC 20 August 2006 (20 h) (Figs. 8e,f), although the ground-relative streamlines exhibit a fully

closed circulation (Figs. 8a–c). Moreover, the low- and midlevel streamlines are intersected with high angles, except at the northern end of the linear MCS. Given the conservative property of absolute vorticity, some LVs may be advected out of the convective regions (or escaped from the AEW pouch region) to the north-northeast, even considering some frictional convergence toward lower MSLP. Notably, the two LVs in the vicinity of MVs A and B, labeled “ $d_1$ ” and “ $d_2$ ” (Figs. 8e,f and 9a–c), respectively, move out of the display domains during the period 0600–1200 UTC 21 August 2006 (30–36 h), when the curvatures of the low-level comoving streamlines are markedly reduced (Figs. 9b,c), as is the case for LV “ $d_3$ ” associated with MV C (Figs. 9b–e). This implies that the LVs could contribute to TCG only when they are secured within a vertically coherent vortex circulation, as occurred during the genesis of Hurricane Julia (2010) from an AEW shown by Cecelski and Zhang (2013). This scenario differs from the other TCG cases, in which the bottom-up growth of cyclonic vorticity dominates (e.g., Zhang and Bao 1996; Montgomery et al. 2012). Similarly, only those midlevel vorticity patches within the AEW pouch could be

eventually converged into the AEW's inner-core region, contributing to the genesis of Debby, as will be shown next.

Figure 9 shows clearly that the formation of TD Debby coincides with the merging of MVs A–C, which are secured within the midlevel pouch. First, note that after their formation, the three MVs are not individually related to their initiating LVs because of the different flow patterns in which they are embedded. Second, as compared to the other two MVs, MV A is nearly stationary over the 36-h period prior to TD, because it is predominantly located in the wave pouch's inner-core region. But it becomes weaker and more elongated as it is advected cyclonically rearward away from the leading convergence zone (Figs. 8 and 9a–d). Third, MV B, located on the opposite (southern) side of MV A in the AEW pouch at 0000 UTC 21 August 2006 (24 h), intensifies significantly via stretching, as indicated by pronounced intersecting streamlines, during the following 18 h as it is advected cyclonically northeastward into the leading confluence zone to the east. This leads to its quick merging with the trailing cyclonic vorticity field of MV A. A similar scenario exists for MV C after it moves into the southwesterly confluence zone (Figs. 9c,d). TD Debby forms after the three MVs are mostly merged into a mesovortex (centered at MV B) carrying intense cyclonic vorticity in the core region with remnant trailing patches of vorticity bands extending cyclonically outward (Fig. 9e). Strictly speaking, more vorticity patches from B and C are merged with a small trailing portion from A, as will be further detailed later. Of relevance is that even though a surface cyclone of intense vorticity associated with  $d_1$  develops with compact cyclonic streamlines and well-organized convection at 0000 UTC 21 August 2006 (24 h) (Figs. 6d and 9a), TCG could not be triggered because of the lack of its collocation with an MV.

Note the convective generation of new LVs near the pouch core region with increased convergence toward an LV near MV B after 1200 UTC 21 August 2006 (36 h), and the development of a comoving closed circulation at the time of genesis (Figs. 9d–f). Specifically, the newly generated LVs contribute to the genesis of Debby, given the existence of bottom-up development (Zhang and Bao 1996; Montgomery et al. 2006) and their collocations with the midlevel disturbances. Indeed, the TD stage is reached at 0000 UTC 22 August 2006 (48 h) as one intense LV, with the peak relative vorticity exceeding  $10^{-3} \text{ s}^{-1}$  resulting from the congregation of a few LVs during the period from 1200 UTC 21 August (36 h) to 0000 UTC 22 August 2006 (48 h) (Figs. 9c–e), becomes more vertically coherent with the merged midlevel mesovortex. Note that the

peak LV intensity is nearly one order of magnitude greater than the merged midlevel mesovortex. A corresponding surface mesolow is also well developed at this time, claiming the formation of TD Debby, as will be shown in the next section. The associated cyclonic circulation grows in both intensity and area coverage from this time on (cf. Figs. 5a and 9e,f). One may also note a convectively generated low-level vorticity band to the south, but it contributes little to the amplification of the storm, as it is located outside the low-level closed Lagrangian circulation.

Before discussing the roles of the MVs and their interaction with LVs in the genesis of Debby, it is desirable to examine the nonlinear response of the low-level circulations to the presence of the three elevated MVs. This can be achieved by applying a piecewise PV inversion algorithm, which has been demonstrated by Davis and Emanuel (1991) and Kieu and Zhang (2010) for an extratropical cyclone and a tropical cyclone, respectively. In this study, three PV pieces associated with MVs A, B, and C are obtained following the methodology developed by Kieu and Zhang (2010). Specifically, the associated PV anomalies (PVAs) are first isolated after subtracting a basic state that is defined as the azimuthal averaged PV field (i.e.,  $\overline{PV}$ ) centered at the AEW's 600-hPa circulation in the comoving framework (viz.,  $PVAs = PV - \overline{PV}$ ) where PVAs include those associated with MVs A, B, and C, plus all the remaining portion over the PV inversion domain. The three PVAs are subjectively partitioned, respectively, in vertical columns with the radius of 50 km centered near individual maximum PVAs at 600 hPa; they are referred to as  $q'_A$ ,  $q'_B$ , and  $q'_C$ , respectively.

Figure 10 shows the contributions of MVs A, B, and C to the total MSLP perturbations at two time levels using the piecewise PV inversion algorithm following Kieu and Zhang (2010). It is evident from Fig. 10c that the PV and PVA associated with each MV can be easily identified with peak magnitudes located in the midtroposphere near the melting level (Kieu and Zhang 2009), albeit with cyclonic vorticity magnitudes less than that associated with LVs (cf. Figs. 10c and 8e,f). Additionally, the peak PV of each MV occurs in the stratiform region, where upward motion is, on average, relatively weak (cf. Figs. 10c and 8j). Of relevance is that the inverted MSLP fall is concentrated closely beneath each PVA, with the peak values of 1–2 hPa, although the influences spread over an area at or exceeding roughly  $400 \text{ km} \times 400 \text{ km}$  (Figs. 10a,b). The MSLP fall associated with MV A appears to dominate during the genesis of Debby, especially at 1800 UTC 21 August 2006 (42 h) (Fig. 10b). Obviously, it has the strongest PV (greater than 4 PV units;  $1 \text{ PVU} = 10^{-6} \text{ K kg}^{-1} \text{ m}^2 \text{ s}^{-1}$ ) and is situated persistently near the AEW pouch center. In

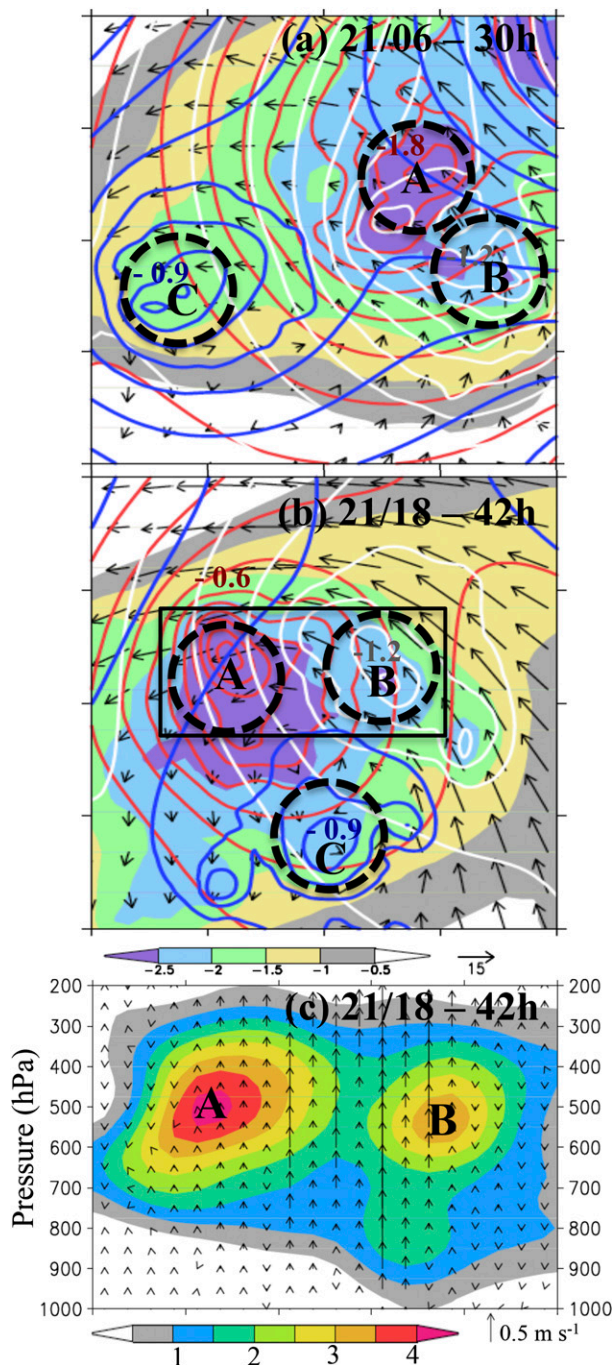


FIG. 10. Horizontal distribution of the piecewise PV-inverted sea level pressure perturbations from the total (shaded), MV A (red), MV B (white), and MV C (blue) contoured at an interval of 0.3 hPa, superimposed with wind vectors at 600 hPa from (a) 30- and (b) 42-h simulations over a domain size of  $400 \text{ km} \times 400 \text{ km}$  centered at the AEW pouch core. Dashed black circles represent the size of PV pieces associated with each MV. (c) As in (b), but for the vertical cross section of the 100-km meridionally averaged PV (shaded; PVU) over the rectangle given in (b). Intervals marked on the frames of (a) and (b) denote 100-km distances.

fact, the MV A-induced MSLP fall coincides well with the total MSLP fall (shaded in Figs. 10a and 10b) induced by all the MVs, with the peak value of 2.5–3 hPa, nearly identical to the MSLP perturbation of the developing depression (Fig. 5a).

The intersections of MSLP isobars induced by the three MVs indicate the importance of vortex–vortex interaction, in addition to the previously mentioned vorticity advection by southwesterly converging flows within the larger-scale intensifying AEW circulation in reaching Debby’s TD stage. That is, MVs A, B, and C tend to be advected cyclonically toward the wave-pouch core region under the influence of midlevel confluence or convergence (in the areas with intersecting streamlines). As they become closer to each other [e.g., at 1800 UTC 21 August 2006 (42 h); Figs. 9d and 10b] the meso- $\beta$ -scale vortex–vortex interaction in the presence of midlevel convergence (toward the corresponding lower pressure centers) tends to accelerate their merging into the pouch core region, eventually culminating in a notable bull’s eye of intense cyclonic vorticity at the TD stage (Fig. 9e).

Given the contributions of the MVs to the MSLP perturbations, we may now examine the interaction of the MVs and LVs during a 5-h TCG period prior to TD. Figures 11a–c show the presence of two major convergence zones that are associated with the linear rainband near  $10^\circ\text{N}$  and the MCS/MV B to the north, respectively. Again, convectively generated LVs, including  $d_3$ , along the linear rainband contribute little to the genesis of Debby despite their development within a closed ground-relative circulation at 950 hPa during the pre-TD period (Figs. 11d–f and 12a,b). Only one LV, located between MVs B and C, is seen to be collocated with the midlevel mesovortex after forming a closed low-level Lagrangian circulation. Vertical cross sections through this LV and MV B show that the latter takes place between two more intense convergence (and convective) regions at 1800 UTC 21 August 2006 (42 h): one is associated with the LV, and the other accounts for the formation of an intense vorticity patch to the north of MV B at 2200 UTC 21 August 2006 (46 h) (Fig. 11f). This vorticity patch, coinciding with a convective segment in the north, appears to be quasi stationary, and it is not merged with the other MVs at the TD stage (cf. Figs. 11c,f and 12a,b). Based on the PV-inverted MSLP perturbation, MV B must help induce the convergence underneath it in the PBL between the abovementioned two convergence regions, though this is not possible to quantify. A further analysis of the hourly plots [between 2200 UTC 21 August (46 h) and 0000 UTC 22 August 2006 (48 h)] reveals that the TD stage is reached after the LV and midlevel mesovortex are collocated, with an intense low-level convergence zone associated with a central

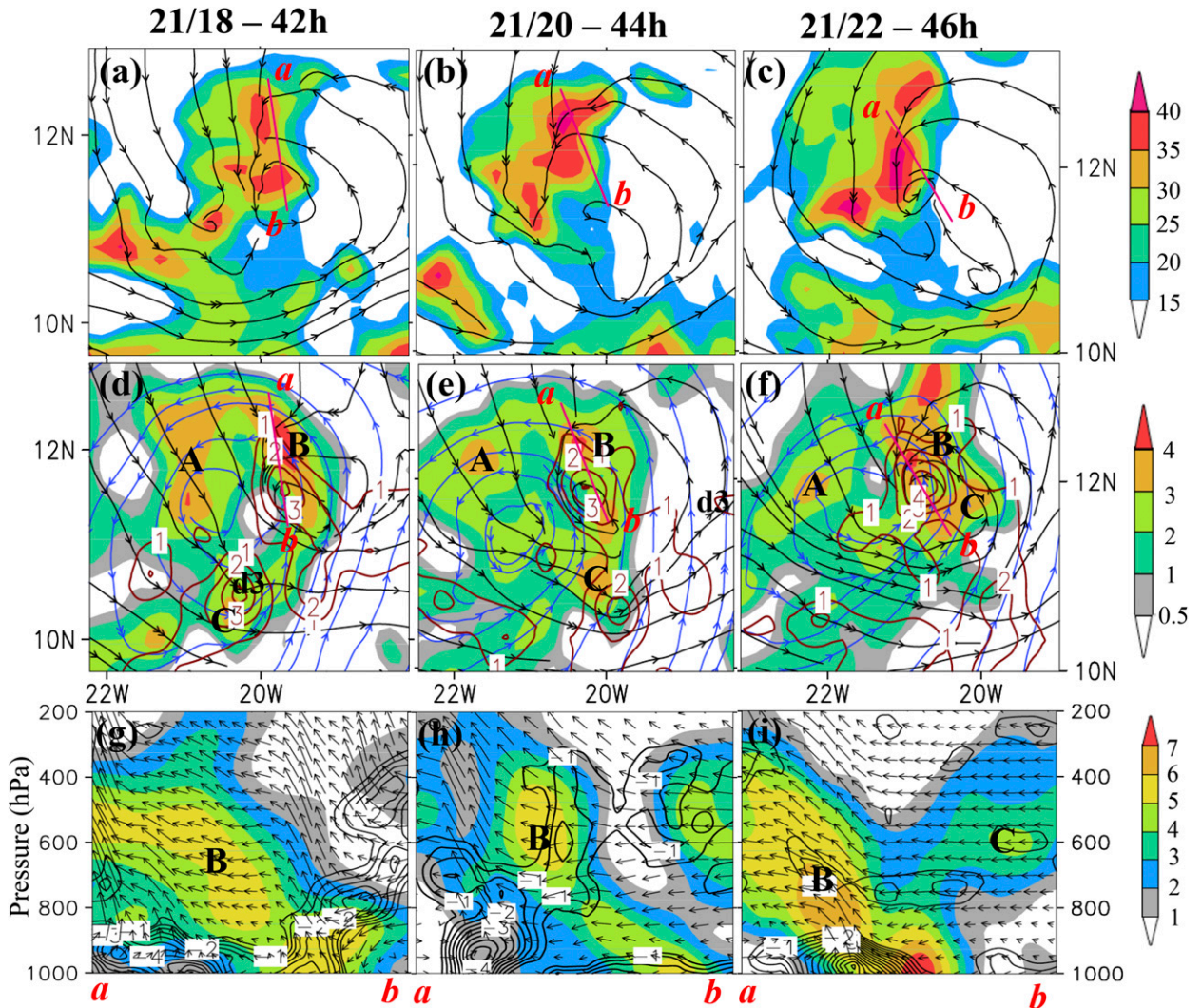


FIG. 11. As in Fig. 8, except from the (a),(d),(g) 42-, (b),(e),(h) 44-, and (c),(f),(i) 46-h simulations over much smaller domains. Symbol  $d_3$  denotes the LV that eventually escaped from the AEW pouch region.

convective segment that is aided by the MV B-induced convergence (Figs. 11c,i and 12a,b). The significance of the resulting convergence in facilitating rapid vorticity growth can be seen from Fig. 12c, which shows a meso- $\beta$ -scale (about 60 km in diameter) robust vortex that is characterized by the peak relative vorticity exceeding  $15 \times 10^{-4} \text{ s}^{-1}$  in the PBL with pronounced upward motion and precipitation in the core region. This vorticity amplitude nearly doubles that at 1 h earlier. This vortex grows further in intensity, depth, and size to form TD Debby 1 h later (Fig. 12d), with its peak vorticity exceeding  $21 \times 10^{-4} \text{ s}^{-1}$ . It continues to expand slowly as it deepens to TS (cf. Figs. 9e,f); the simulated small storm size is in agreement with that seen in satellite imagery (Figs. 6e–f).

It is necessary to discuss how the midlevel vorticity evolves during the final 6-h pre-TD period. An

examination of the model output shows that the peak vorticity of MV B at 600 hPa grows slowly from  $6 \times 10^{-4}$  to  $7 \times 10^{-4} \text{ s}^{-1}$ , mostly through stretching between the 42- and 46-h simulations, as also indicated by Figs. 11g–i; these values are close to the corresponding peaks of  $6 \times 10^{-4}$ – $8 \times 10^{-4} \text{ s}^{-1}$  associated with the LV to the southeast. Subsequently, the peak vorticity at 600 hPa increases to  $8 \times 10^{-4} \text{ s}^{-1}$  at 47 h (i.e., shortly after merging) and rapidly to  $14 \times 10^{-4} \text{ s}^{-1}$  at 48 h (Figs. 12c,d). Clearly, the upward vorticity advection must play a role in accelerating the midlevel vorticity growth during the final 1–2-h merging stage. However, the vorticity growth in the central column may be slowed after 48 h because of the development of subsiding motion and weak divergence (Fig. 12d); the latter will be discussed in the next section.

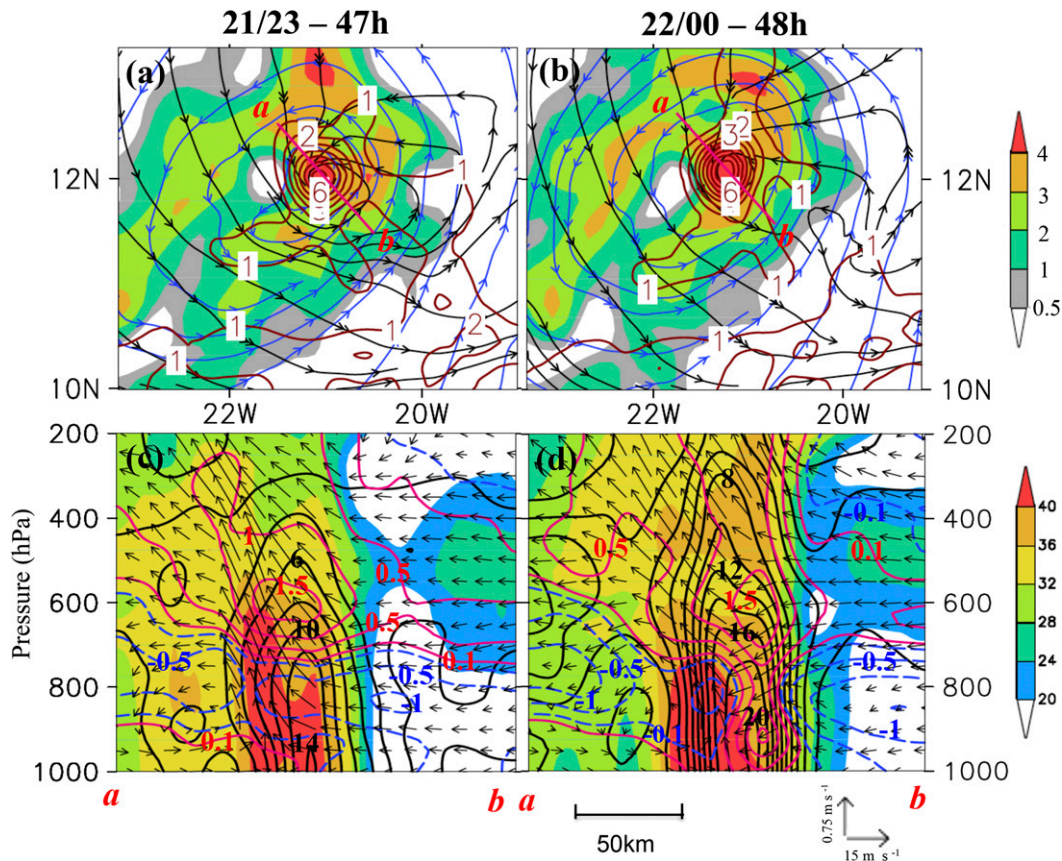


FIG. 12. (a),(b) As in Figs. 8d–f, but for the 47- and 48-h simulations, respectively, over much smaller domains. (c),(d) Vertical cross section of relative vorticity (black contours; interval of  $2 \times 10^{-4} \text{ s}^{-1}$ ) and temperature deviation (contoured at  $\pm 0.1^\circ$ ,  $\pm 0.5^\circ$ ,  $\pm 1^\circ$ , and  $\pm 1.5^\circ\text{C}$ ; positive is red solid, negative is blue dashed), radar reflectivity (dBZ; shaded), and in-plane flow vectors along line a–b in (a) and (b) from the 47- and 48-h simulations, respectively. Temperature deviations are calculated by subtracting the corresponding level-averaged values over the same length as that used in Fig. 13a. See Fig. 13b for the cross-sectional window size used in (d).

## 5. Thermodynamic transformation

TCG from AEWs involves both the spinup of low-level cyclonic flows and the thermodynamic transformation from a cold to a warm core at the TC center. For this purpose, Fig. 13 compares the vertical cross-sectional structures of relative vorticity and temperature deviations at the TD stage, 24 h prior and after. The AEW at 0000 UTC 21 August 2006 (24 h) is characterized by the northwestward-tilted vorticity, which is peaked near 600 hPa, albeit associated mostly with MV A, with warm (weak ascending) air above and cold (weak descending) air below (Fig. 13a). These vertical vorticity and thermal structures are similar to those occurring at the model initial time (Figs. 2b, 3a). Of interest is that these AEW structures could still be more or less seen at the TD stage (cf. Figs. 13a and 13b).

Because of its small size, the vertical vortex structures given in Fig. 13b are replotted in Fig. 12d but with a

small window. Despite the generation of a robust vortex, we could still see a cold layer below with a warm column above 700 hPa even at 2300 UTC 21 August 2006 (47 h) (Fig. 12c). This warmth may be attributed partly to the balanced portion of the midlevel pouch, like that at 0000 UTC 21 August 2006 (24 h) (Fig. 13a), and partly to the residual between diabatic heating and adiabatic cooling in updrafts and compensating subsidence warming in downdrafts, as shown by Cecelski and Zhang (2013). Of importance is the removal of the cold dome near the vortex center, albeit narrow in scale, when a TD stage is reached at 0000 UTC 22 August 2006 (48 h) (Fig. 12d). This removal must be performed by subsidence warming, as can be seen from the vortex-scale downdrafts below 550 hPa with the peak amplitude of  $0.75 \text{ m s}^{-1}$  at 750 hPa. The radial extent of rainfall also decreases (cf. Figs. 12c and 12d). The subsidence does not seem to be triggered by evaporative cooling, because the vortex is nearly saturated. This subsidence may be induced by the

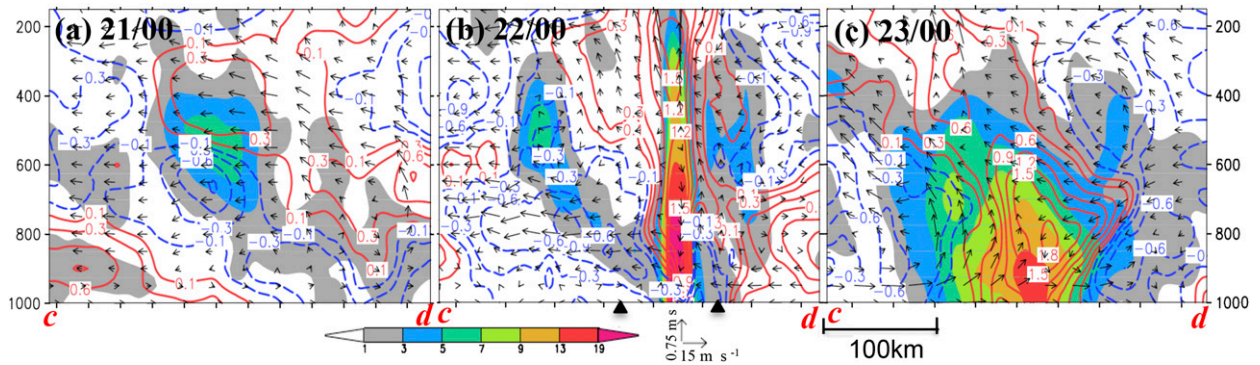


FIG. 13. Vertical cross section of relative vorticity (shaded;  $10^{-4} \text{ s}^{-1}$ ), temperature deviations (contours; interval of  $0.3^\circ\text{C}$ ), and in-plane flow vectors through the vorticity centers of the AEW pouch and Debby along line c–d in (a) Fig. 9a, (b) Fig. 9e, and (c) Fig. 6c from the 24-, 48-, and 72-h simulations, respectively. Temperature deviations are calculated by subtracting the corresponding level-averaged values. Two triangles at the bottom of (b) are marked to denote the cross-sectional window range used in Fig. 12d.

dynamical perturbation pressure gradient force in the vertical due to rapid rotation, like a mature TC, as discussed by Zhang et al. (2000), which is then enhanced by melting and evaporative cooling. This thermodynamic transformation process appears to differ from the advective process by subvortices shown by Zhang and Bao (1996) and the sensible heating from the underlying warm ocean hypothesized by Bister and Emanuel (1997). This difference appears to be attributable to the development of intense rotation in such a small-sized vortex.

The weak subsiding motion in the core region does not extend to the upper troposphere until Debby reaches its TS stage (Fig. 13c). At this stage, the size of the simulated Debby in terms of cyclonic vorticity has nearly doubled (i.e., from about 60 to 120 km in diameter) during the 12-h period (cf. Figs. 13b and 13c), which is similar to the growth of its warm-core structure.

Figure 14 shows time series of the vertical profiles of temperature changes at the AEW pouch center with respect to the model initial time. Because of the 12–24-h nudging simulation used prior to the model initial time, upper-level warming in the pouch core begins shortly after the model integration. Two vertical warming modes start to appear at 1500 UTC August 2006 (15 h): a major peak near 300 hPa and a secondary peak in the 700–800-hPa layer. The two peaks are clearly separated by melting-induced cooling beneath the  $0^\circ\text{C}$  level. Zhang and Zhu (2012) examined the genesis of Typhoon Chanchu (2006), in which the vorticity–thermal structures are also vertically tilted. Only a single warming mode, peaked in the 400–500-hPa layer, is found. TCG in the case of Chanchu occurs as the tilted structures become more vertically coherent (Hogsett and Zhang 2010). In the present case, both the upper- and lower-level warming increases in depth and amplitude near

1200 UTC 21 August 2006 (36 h), lowering hydrostatically pressure in the layers below, especially MSLP, which facilitates the formation of TD Debby 12 h later. The lowered pressure below the upper-level warming is consistent with increased midtropospheric circulations (cf. Figs. 14 and 7a), when gradient wind balance is considered.

The time series of local VWS profile in Fig. 14 shows the presence of weak VWS of about  $1 \text{ s}^{-1}$  above 700 hPa, which is favorable for maintaining the upper-level warmer air, as discussed by Zhang and Zhu (2012). In contrast, significant VWS (up to  $8 \text{ s}^{-1}$ ) occurs in the lowest 300 hPa of the troposphere, dominating the magnitude of deep-layered VWS shown in Fig. 5b. The

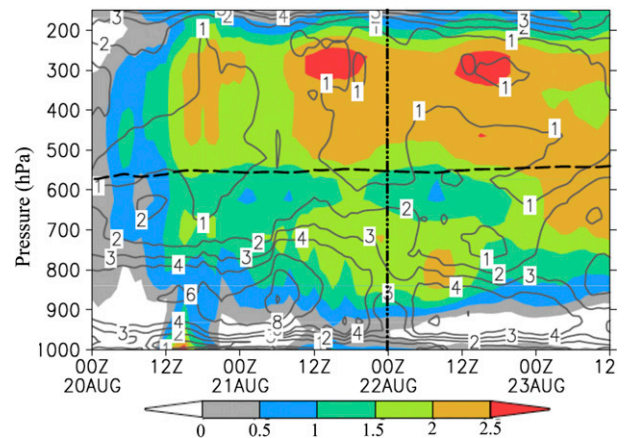


FIG. 14. Time–height cross section of the differenced temperature with respect to its initial value (shaded;  $^\circ\text{C}$ ) and vertical wind shear (contours; interval of  $10^{-3} \text{ s}^{-1}$ ), which are obtained by  $600 \text{ km} \times 600 \text{ km}$  area average at the AEW pouch center during the 84-h simulations, valid from 0000 UTC 20 Aug to 1200 UTC 23 Aug 2006. Dashed lines denote the melting level, and dotted-dashed lines represent the time of the TD stage.

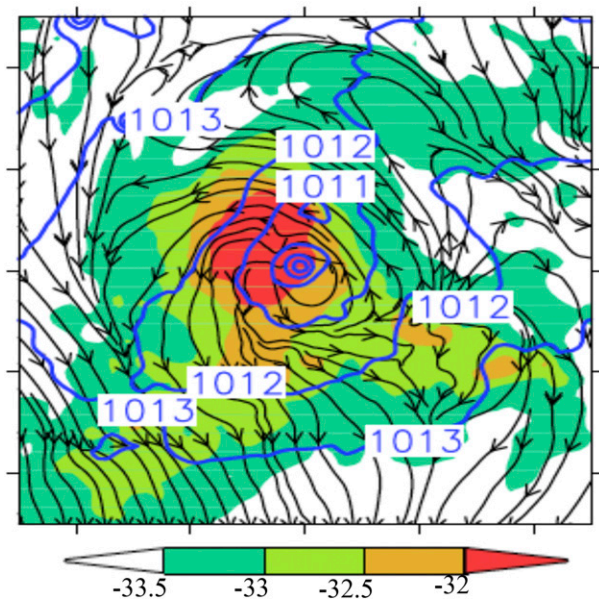


FIG. 15. Horizontal distribution of the comoving streamlines and temperatures (shading;  $^{\circ}\text{C}$ ), superimposed with MSLP at an interval of 1 hPa over an area of  $1000\text{ km} \times 1000\text{ km}$  at 250 hPa from the 48-h simulations. Tick marks on the frame denote 200-km distances.

marked drop in the layered VWS coincides with the pronounced increase in the upper- and lower-level warming, indicating the development of more deep convection in the pouch core region (Figs. 11a–c). Additionally, a significant portion of this VWS is caused by wind directional differences between the AEW's mid- and lower-level circulations (Fig. 9). The directional differences become smaller after reaching TD, as the rotational flows in the core region become more vertically coherent. On the other hand, the lower-level VWS is less detrimental to TCG because of the presence of larger inertial stability associated with the LVs, and it may even be favorable for TCG (Bracken and Bosart 2000).

Figure 15 shows the presence of meso- $\alpha$ -scale warmer air at 250 hPa that is closely related to a well-defined surface mesolow at the TD stage, and it should be also hydrostatically related to the enhancement of the mid-level marsupial pouch. This implies that the upper-level processes producing the mesoscale warming (e.g., outflow, VWS, and inertial stability) must play an important role in TCG. This warm air mass is more or less protected by convectively generated outflow aloft (Fig. 15). This is favored by the presence of weak VWS (Zhang and Chen 2012; Zhang and Zhu 2012) in the present case. Clearly, this surface mesolow would help enhance larger-scale mass and moisture convergence, facilitating the generation and intensification of LVs, and enhancing

the cyclonic rotation at the storm scale. Note that, strictly speaking, the upper-level processes should also include convective overshooting into the lower stratosphere, forming a local cold dome with a high pressure anomaly below (Fritsch and Brown 1982). It is essentially this high pressure anomaly that drives the upper-level outflow spreading warm air outward to the mesoscale, while the cold air above subsides slowly.

## 6. Summary and conclusions

In this study, the genesis of Tropical Storm Debby (2006) within an AEW is examined, with more focus on the generation of MVs and their interaction with LVs, using a cloud-resolving simulation of the storm with the finest grid size of 1.33 km. A large-scale analysis reveals that TCG takes place in the AEW pouch core region with favorable larger-scale conditions, such as reduced VWS, a midlevel cyclonic circulation forming a well-defined pouch, and a moist environment generated by prior convection. After verifying the model simulation of the storm against available observations, the high-resolution model output is used herein to examine the mesoscale processes leading to the genesis of Debby. Results show the development of two rainbands within the AEW before moving offshore, and the subsequent bottom-up generation of several meso- $\beta$ -scale MVs and convectively generated LVs along the rainbands. The MVs are then advected into the trailing stratiform region by front-to-rear ascending flows in the rainbands, where they are enhanced mostly through vortex stretching of the absolute vorticity associated with convergence near the melting level.

Figure 16 provides a conceptual model showing the subsequent evolution of three major MVs (A, B, and C) and their interaction within the midlevel pouch, LVs ( $d_1$ ,  $d_2$ , and  $d_3$ ) and lower-level comoving circulations, leading to the genesis of Debby. The MVs, which are secured within the AEW pouch, are phase shifted from the LVs during the early stages (Fig. 16a). They are intensifying while circling into the pouch core region under the influence of converging flows, especially when moving along the rainband. Because of the different circulation structures, the MVs are displaced along different paths, after their formation, from the corresponding LVs. As they become closer to each other (Fig. 16b), the meso- $\beta$ -scale vortex–vortex interaction in the presence of midlevel convergence toward the corresponding lower pressure centers tends to accelerate their merging into the pouch core region, eventually culminating in a notable bull's eye of one midlevel mesovortex at the TD stage (Fig. 16c). In contrast, the low-level comoving flows are opened as a wave trough at

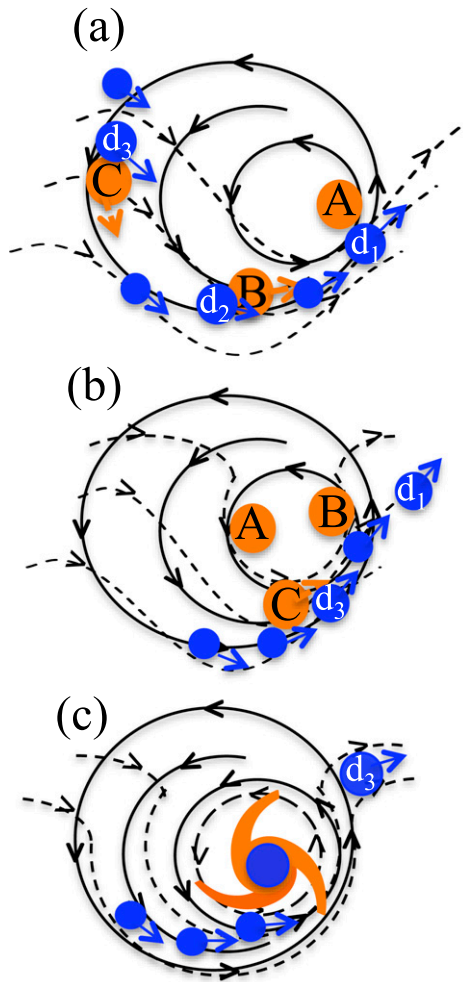


FIG. 16. A conceptual model describing the evolution of MVs (orange circles), LVs (smaller blue circles), and midlevel (solid) and low-level (dashed) comoving streamlines during the (a) early, (b) near-TD, and (c) TD stages of Debby. Larger blue circles denote major LVs discussed in the text. Symbols  $d_1$ ,  $d_2$ , and  $d_3$  denote the LVs that eventually escaped from the AEW pouch region. Arrows indicate the directions of movements of individual vortices.

the earlier stages, so the LVs tend to be advected out of the rainband regions to the north-northeast (Figs. 16a,b). This indicates that these LVs could not contribute to TCG, unlike those shown in the previous TCG studies, in which the bottom-up growth of cyclonic vorticity dominates. So, LVs can contribute to TCG only after a closed low-level Lagrangian circulation enclosing them is developed and becomes vertically coherent with the midlevel pouch. An application of the piecewise PV inversion to the MVs reveals their important roles in helping induce the closed low-level circulation and their interactions with LVs. It is clear that TD Debby is formed with a well-defined surface mesolow when the midlevel mesovortex is collocated with a major LV and a

convection-induced intense convergence zone in the PBL; a similar process occurs for the cores of the mid- and low-level closed Lagrangian circulations (Fig. 16c). Again, convectively generated vortices outside low-level closed circulations contribute little to the amplification of Debby.

The thermodynamic transformation of the vertically tilted AEW with warm air above a cold dome to TD Debby is examined. Results show the dominance of upward motion in the vortex core region with a warm column above 700 hPa and a cold layer below at the time of merging. A low-level cold column in the core is removed by descending motion as the vortex intensifies rapidly after the merging. As a result, a meso- $\beta$ -scale deep-tropospheric warm column is formed at the TD stage and expands from about 60 to over 120 km in diameter as the vortex intensifies into a TS. This transformation process appears to differ from that revealed in previous studies because of the development of intense cyclonic vorticity in such a small-sized TS. The present work also confirms the roles of upper-level warming in hydrostatically maintaining the midlevel pouch, increasing midtropospheric circulations, and producing meso- $\alpha$ -scale MSLP falls, thereby facilitating the low-level storm-scale convergence, the growth of LVs, and the formation of Debby.

In summary, the key elements in the sequence of TCG in the present case include: (i) convectively generated upper-level warming and its roles in maintaining a midlevel pouch and inducing meso- $\alpha$ -scale MSLP falls, (ii) the bottom-up generation of MVs and convectively generated LVs as well as their growth in mesoscale converging flows, (iii) merging of the MVs within the pouch but escaping of the LVs from it because of the presence of a low-level open trough, (iv) the development of a closed low-level Lagrangian circulation and likely congregation of newly generated LVs within it, and (v) the collocation of the midlevel merged mesovortex with the congregated LV and a convective zone with intense convergence in the PBL. It appears that this sequence of events tends to slow the rate of TCG, as compared to other cases, in which the low- to midlevel storm-scale circulations are more vertically coherent. The results may also help explain why many tropical disturbances could not develop into TS intensity, whereas some could. Clearly, to generalize the above findings, more TCG cases associated with AEWs should be studied in the future.

*Acknowledgments.* We wish to thank Dr. Zhuo Wang and the two anonymous reviewers for their constructive comments that have helped improve the quality of this manuscript. This work was supported by the Priority Academic Program Development of Jiangsu Higher

Education Institutions (PAPD), NSF Grant ATM0758609, and ONR Grant N000141410143. The WRF Model integration was completed with the computational support of the National Center for Atmospheric Research, which is sponsored by the National Science Foundation.

## REFERENCES

- Avila, L. A., and R. J. Pasch, 1992: Atlantic tropical systems of 1991. *Mon. Wea. Rev.*, **120**, 2688–2696, doi:10.1175/1520-0493(1992)120<2688:ATSO>2.0.CO;2.
- Biggerstaff, M. I., and R. A. Houze Jr., 1991: Kinematic and precipitation structure of the 10–11 June 1985 squall line. *Mon. Wea. Rev.*, **119**, 3034–3065, doi:10.1175/1520-0493(1991)119<3034:KAPSOT>2.0.CO;2.
- Bister, M., and K. A. Emanuel, 1997: The genesis of Hurricane Guillermo: TEXMEX analysis and a modeling study. *Mon. Wea. Rev.*, **125**, 2662–2682, doi:10.1175/1520-0493(1997)125<2662:TGOHGT>2.0.CO;2.
- Bracken, W. E., and L. F. Bosart, 2000: The role of synoptic-scale flow during tropical cyclogenesis over the North Atlantic Ocean. *Mon. Wea. Rev.*, **128**, 353–376, doi:10.1175/1520-0493(2000)128<0353:TROSSF>2.0.CO;2.
- Cecelski, S., and D.-L. Zhang, 2013: Genesis of Hurricane Julia (2010) from an African easterly wave: LVs and upper-level warming. *J. Atmos. Sci.*, **70**, 3799–3817, doi:10.1175/JAS-D-13-043.1.
- , —, and T. Miyoshi, 2014: Genesis of Hurricane Julia (2010) within an African easterly wave: Developing and non-developing members from WRF-LETKF ensemble forecasts. *J. Atmos. Sci.*, **71**, 2763–2781, doi:10.1175/JAS-D-13-0187.1.
- Charney, J. G., and M. E. Stern, 1962: On the stability of internal baroclinic jets in a rotating atmosphere. *J. Atmos. Sci.*, **19**, 159–172, doi:10.1175/1520-0469(1962)019<0159:OTSOIB>2.0.CO;2.
- Chen, T.-C., S.-Y. Wang, and A. J. Clark, 2008: North Atlantic hurricanes contributed by African easterly waves north and south of the African easterly jet. *J. Climate*, **21**, 6767–6776, doi:10.1175/2008JCLI2523.1.
- Chiao, S., and G. S. Jenkins, 2010: Numerical investigations on the formation of Tropical Storm Debby during NAMMA-06. *Wea. Forecasting*, **25**, 866–884, doi:10.1175/2010WAF2222313.1.
- Cornforth, R. J., B. J. Hoskins, and C. D. Thorncroft, 2009: The impact of moist processes on the African easterly jet–African easterly wave system. *Quart. J. Roy. Meteor. Soc.*, **135**, 894–913, doi:10.1002/qj.414.
- Davis, C. A., and K. Emanuel, 1991: Potential vorticity diagnostics of cyclogenesis. *Mon. Wea. Rev.*, **119**, 1929–1953, doi:10.1175/1520-0493(1991)119<1929:PVDOC>2.0.CO;2.
- Dunkerton, T. J., M. T. Montgomery, and Z. Wang, 2009: Tropical cyclogenesis in a tropical wave critical layer: Easterly waves. *Atmos. Chem. Phys.*, **9**, 5587–5646, doi:10.5194/acp-9-5587-2009.
- Frank, N. L., 1970: Atlantic tropical systems of 1969. *Mon. Wea. Rev.*, **98**, 307–314, doi:10.1175/1520-0493(1970)098<0307:ATSO>2.3.CO;2.
- Franklin, J. L., 2006: Tropical cyclone report: Tropical Storm Debby. National Hurricane Center Tech. Rep. AL052006, 9 pp. [Available online at [http://www.nhc.noaa.gov/data/tcr/AL052006\\_Debby.pdf](http://www.nhc.noaa.gov/data/tcr/AL052006_Debby.pdf).]
- Fritsch, J. M., and J. M. Brown, 1982: On the generation of convectively driven mesohighs aloft. *Mon. Wea. Rev.*, **110**, 1554–1563, doi:10.1175/1520-0493(1982)110<1554:OTGOCD>2.0.CO;2.
- Goldenberg, S. B., and L. J. Shapiro, 1996: Physical mechanisms for the association of El Niño and West African rainfall with Atlantic major hurricane activity. *J. Climate*, **9**, 1169–1187, doi:10.1175/1520-0442(1996)009<1169:PMFTAO>2.0.CO;2.
- Gray, W. M., 1968: Global view of the origin of tropical disturbances and storms. *Mon. Wea. Rev.*, **96**, 669–700, doi:10.1175/1520-0493(1968)096<0669:GVOTOO>2.0.CO;2.
- , 1985: Tropical cyclone climatology. WMO Tech. Doc. WMO/TD-72, Vol. 1, 145 pp.
- Hendricks, E. A., M. T. Montgomery, and C. A. Davis, 2004: The role of “vortical” hot towers in the formation of Tropical Cyclone Diana (1984). *J. Atmos. Sci.*, **61**, 1209–1232, doi:10.1175/1520-0469(2004)061<1209:TROVHT>2.0.CO;2.
- Hogsett, W., and D.-L. Zhang, 2010: Genesis of Typhoon Chanchu (2006) from a westerly wind burst associated with the MJO. Part I: Evolution of a vertically tilted precursor vortex. *J. Atmos. Sci.*, **67**, 3774–3792, doi:10.1175/2010JAS3446.1.
- , and —, 2011: Genesis of Typhoon Chanchu (2006) from a westerly wind burst associated with the MJO. Part II: Roles of deep convection in tropical transition. *J. Atmos. Sci.*, **68**, 1377–1396, doi:10.1175/2010JAS3512.1.
- Hong, S.-Y., Y. Noh, and J. Dudhia, 2006: A new vertical diffusion package with an explicit treatment of entrainment processes. *Mon. Wea. Rev.*, **134**, 2318–2341, doi:10.1175/MWR3199.1.
- Hopsch, S., C. D. Thorncroft, K. Hodges, and A. Aiyyer, 2007: West African storm tracks and their relationship to Atlantic tropical cyclones. *J. Climate*, **20**, 2468–2483, doi:10.1175/JCLI4139.1.
- , —, and K. R. Tyle, 2010: Analysis of African easterly wave structures and their role in influencing tropical cyclogenesis. *Mon. Wea. Rev.*, **138**, 1399–1419, doi:10.1175/2009MWR2760.1.
- Houze, R. A., Jr., S. A. Rutledge, M. I. Biggerstaff, and B. F. Smull, 1989: Interpretation of Doppler weather radar displays in midlatitude mesoscale convective system. *Bull. Amer. Meteor. Soc.*, **70**, 608–619, doi:10.1175/1520-0477(1989)070<0608:IODWRD>2.0.CO;2.
- , W.-C. Lee, and M. M. Bell, 2009: Convection contribution to the genesis of Hurricane Ophelia (2005). *Mon. Wea. Rev.*, **137**, 2778–2800, doi:10.1175/2009MWR2727.1.
- Kain, J. S., 2004: The Kain–Fritsch convective parameterization: An update. *J. Appl. Meteor.*, **43**, 170–181, doi:10.1175/1520-0450(2004)043<0170:TKCPAU>2.0.CO;2.
- Kieu, C. Q., and D.-L. Zhang, 2009: Genesis of Tropical Storm Eugene (2005) from merging vortices associated with ITCZ breakdowns. Part II: Roles of vortex merger and ambient potential vorticity. *J. Atmos. Sci.*, **66**, 1980–1996, doi:10.1175/2008JAS2905.1.
- , and —, 2010: A piecewise potential vorticity inversion algorithm and its application on hurricane inner-core anomalies. *J. Atmos. Sci.*, **67**, 2616–2631, doi:10.1175/2010JAS3421.1.
- Lin, Y.-L., L. Liu, G. Tang, J. Spinks, and W. Jones, 2013: Origin of the pre-tropical storm Debby (2006) African easterly wave-mesoscale convective system. *Meteor. Atmos. Phys.*, **120**, 123–144, doi:10.1007/s00703-013-0248-6.
- Mlawer, E. J., S. J. Taubman, P. D. Brown, M. J. Iacono, and S. A. Clough, 1997: Radiative transfer for inhomogeneous atmospheres: RRTM, a validated correlated-k model for the longwave. *J. Geophys. Res.*, **102**, 16 663–16 682, doi:10.1029/97JD00237.
- Molinari, J., D. Knight, M. Dickinson, D. Vollaro, and S. Skubis, 1997: Potential vorticity, easterly waves, and eastern Pacific tropical cyclogenesis. *Mon. Wea. Rev.*, **125**, 2699–2708, doi:10.1175/1520-0493(1997)125<2699:PVEWAE>2.0.CO;2.
- , D. Vollaro, S. Skubis, and M. Dickinson, 2000: Origins and mechanisms of eastern Pacific tropical cyclogenesis: A

- case study. *Mon. Wea. Rev.*, **128**, 125–139, doi:10.1175/1520-0493(2000)128<0125:OAMOEP>2.0.CO;2.
- Montgomery, M. T., M. E. Nicholls, T. A. Cram, and A. B. Saunders, 2006: A vortical hot tower route to tropical cyclogenesis. *J. Atmos. Sci.*, **63**, 355–386, doi:10.1175/JAS3604.1.
- , Z. Wang, and T. J. Dunkerton, 2010: Coarse, intermediate and high resolution numerical simulations of the transition of a tropical wave critical layer to a tropical storm. *Atmos. Chem. Phys.*, **10**, 10 803–10 827, doi:10.5194/acp-10-10803-2010.
- , and Coauthors, 2012: The Pre-Depression Investigation of Cloud Systems in the Tropics (PREDICT) experiment: Scientific basis, new analysis tools, and some first results. *Bull. Amer. Meteor. Soc.*, **93**, 153–172, doi:10.1175/BAMS-D-11-00046.1.
- Nolan, D. S., 2007: What is the trigger for tropical cyclogenesis? *Aust. Meteor. Mag.*, **56**, 241–266.
- Norquist, D. C., E. E. Recker, and R. J. Reed, 1977: The energetics of African wave disturbances as observed during Phase III of GATE. *Mon. Wea. Rev.*, **105**, 334–342, doi:10.1175/1520-0493(1977)105<0334:TEOWD>2.0.CO;2.
- Ritchie, E. A., and G. J. Holland, 1997: Scale interactions during the formation of Typhoon Irving. *Mon. Wea. Rev.*, **125**, 1377–1396, doi:10.1175/1520-0493(1997)125<1377:SIDTFO>2.0.CO;2.
- Ross, R. S., and T. N. Krishnamurti, 2007: Low-level African easterly wave activity and its relation to Atlantic tropical cyclogenesis in 2001. *Mon. Wea. Rev.*, **135**, 3950–3964, doi:10.1175/2007MWR1996.1.
- , —, S. Pattnaik, and A. Simon, 2009: Energy transformation and diabatic processes in developing and nondeveloping African easterly waves observed during the NAMMA project of 2006. *Wea. Forecasting*, **24**, 1524–1548, doi:10.1175/2009WAF2222235.1.
- Sippel, J. A., S. A. Braun, and C.-L. Shie, 2011: Environmental influences on the strength of Tropical Storm Debby (2006). *J. Atmos. Sci.*, **68**, 2557–2581, doi:10.1175/2011JAS3648.1.
- Skamarock, W. C., and Coauthors, 2008: A description of the Advanced Research WRF version 3. NCAR Tech. Note NCAR/TN-475+STR, 113 pp. [Available online at [http://www2.mmm.ucar.edu/wrf/users/docs/arw\\_v3.pdf](http://www2.mmm.ucar.edu/wrf/users/docs/arw_v3.pdf).]
- Thompson, G., R. M. Rasmussen, and K. Manning, 2004: Explicit forecasts of winter precipitation using an improved bulk microphysics scheme. Part I: Description and sensitivity analysis. *Mon. Wea. Rev.*, **132**, 519–542, doi:10.1175/1520-0493(2004)132<0519:EFOWPU>2.0.CO;2.
- , P. R. Field, R. M. Rasmussen, and W. D. Hall, 2008: Explicit forecasts of winter precipitation using an improved bulk microphysics scheme. Part II: Implementation of a new snow parameterization. *Mon. Wea. Rev.*, **136**, 5095–5115, doi:10.1175/2008MWR2387.1.
- Thorncroft, C. D., and K. Hodges, 2001: African easterly wave variability and its relationship to Atlantic tropical cyclone activity. *J. Climate*, **14**, 1166–1179, doi:10.1175/1520-0442(2001)014<1166:AEWVAI>2.0.CO;2.
- Wang, Z., 2012: Thermodynamic aspects of tropical cyclone formation. *J. Atmos. Sci.*, **69**, 2433–2451, doi:10.1175/JAS-D-11-0298.1.
- , 2014: Characteristics of convective processes and vertical vorticity from the tropical wave to tropical cyclone stage in a high-resolution numerical model simulation of Tropical Cyclone Fay (2008). *J. Atmos. Sci.*, **71**, 896–915, doi:10.1175/JAS-D-13-0256.1.
- , M. T. Montgomery, and T. J. Dunkerton, 2010: Genesis of pre-Hurricane Felix (2007). Part I: The role of the easterly wave critical layer. *J. Atmos. Sci.*, **67**, 1711–1729, doi:10.1175/2009JAS3420.1.
- Zawislak, J., and E. J. Zipser, 2010: Observation of seven African easterly waves in the east Atlantic during 2006. *J. Atmos. Sci.*, **67**, 26–43, doi:10.1175/2009JAS3118.1.
- Zhang, D.-L., and K. Gao, 1989: Numerical simulation of an intense squall line during 10–11 June 1985 PRE-STORM. Part II: Rear inflow, surface pressure perturbations and stratiform precipitation. *Mon. Wea. Rev.*, **117**, 2067–2094, doi:10.1175/1520-0493(1989)117<2067:NSOAI>2.0.CO;2.
- , and N. Bao, 1996: Oceanic cyclogenesis as induced by a meso-scale convective system moving offshore. Part II: Genesis and thermodynamic transformation. *Mon. Wea. Rev.*, **124**, 2206–2226, doi:10.1175/1520-0493(1996)124<2206:OCAIBA>2.0.CO;2.
- , and H. Chen, 2012: Importance of the upper-level warm core in the rapid intensification of a tropical cyclone. *Geophys. Res. Lett.*, **39**, L02806, doi:10.1029/2011GL050578.
- , and L. Zhu, 2012: Roles of upper-level processes in tropical cyclogenesis. *Geophys. Res. Lett.*, **39**, L17804, doi:10.1029/2012GL053140.
- , Y. Liu, and M. K. Yau, 2000: A multiscale numerical study of Hurricane Andrew (1992). Part III: Dynamically induced vertical motion. *Mon. Wea. Rev.*, **128**, 3772–3788, doi:10.1175/1520-0493(2001)129<3772:AMNSOH>2.0.CO;2.
- Zipser, E. J., and Coauthors, 2009: The Saharan air layer and the fate of African easterly waves—NASA’s AMMA field study of tropical cyclogenesis. *Bull. Amer. Meteor. Soc.*, **90**, 1137–1156, doi:10.1175/2009BAMS2728.1.